Tuberculosis susceptibility in genetically diverse mice reveals functional diversity of neutrophils

Marietta M Ravesloot-Chavez[1], Erik Van Dis[2], Douglas Fox[2], Andrea Anaya-Sanchez[1], Scott Espich[3], Xammy Huu Nguyenla[2], Sagar Rawal[2], Helia Samani[2], Mallory Ballinger[4], Henry F Thomas[4], Dmitri I Kotov[2], Russell E Vance[2], Michael W Nachman[4], Sarah A Stanley[2,3]*

[1]Department of Plant and Microbial Biology, University of California, Berkeley, Berkeley, United States; [2]Division of Immunology and Pathogenesis, Department of Molecular and Cell Biology, University of California, Berkeley, Berkeley, United States; [3]School of Public Health, Division of Infectious Disease and Vaccinology, University of California, Berkeley, Berkeley, United States; [4]Department of Integrative Biology, University of California, Berkeley, Berkeley, United States

eLife Assessment

This study provides **valuable** insights into the host's variable susceptibility to *Mycobacterium tuberculosis*, using a novel collection of wild-derived inbred mouse lines from diverse geographic locations, along with immunological and single-cell transcriptomic analyses. While the data are **convincing**, a deeper mechanistic investigation into neutrophil subset functions would have further enhanced the study. This work will interest microbiologists and immunologists in the tuberculosis field.

*For correspondence:
sastanley@berkeley.edu

Abstract Tuberculosis is a heterogeneous disease in humans with individuals exhibiting a wide range of susceptibility. This heterogeneity is not captured by standard laboratory mouse lines. We used a new collection of 19 wild-derived inbred mouse lines collected from diverse geographic sites to identify novel phenotypes during *Mycobacterium tuberculosis* (*Mtb*) infection. Wild-derived mice have heterogeneous immune responses to infection that result in differential ability to control disease at early time points. Correlation analysis with multiple parameters including sex, weight, and cellular immune responses in the lungs revealed that enhanced control of infection is associated with increased numbers of CD4 T cells, CD8 T cells, and B cells. Surprisingly, we did not observe strong correlations between IFN-γ production and control of infection. Although in most lines high neutrophils were associated with susceptibility, we identified a mouse line that harbors high neutrophil numbers yet controls infection. Using single-cell RNA sequencing, we identified a novel neutrophil signature associated with failure to control infection.

Introduction

Mycobacterium tuberculosis (*Mtb*) infection causes a wide range of disease outcomes in humans. Whereas the majority of infected individuals never develop active disease and are able to control infection for their lifetimes, some individuals are highly susceptible to infection and develop active tuberculosis (TB). Patients with active disease show heterogeneity in disease progression. Additionally, the

timing of disease onset after initial infection and disease outcome varies from individual to individual (*Cadena et al., 2017*). This heterogeneity in human responses suggests that TB is a complex genetic disease. Surprisingly, there is only a limited understanding of the genetic factors that contribute to disease progression or control of infection. Indeed, GWAS studies have identified a small number of genetic factors that underlie the variability of responses to *Mtb* in humans including interferon-γ (*IFNG*), interferon-γ receptor (*IFNGR1*), interleukin-12 subunit p40 (*IL12B*), and interleukin-12 receptor b-1 chain (*IL12RB1*) (*Qu et al., 2011*). However, many questions remain regarding what factors determine susceptibility to infection. Despite the clear importance of IFN-γ for control of mycobacterial infection, new vaccine candidates that elicit IFN-γ producing T cells in human volunteers do not elicit complete protection from infection, suggesting that additional protective mechanisms that have yet to be identified may be essential (*Tameris et al., 2013*; *Tait et al., 2019*). Similarly, several immune signatures have been associated with active disease in TB patients, including type I IFN and neutrophils (*Donovan et al., 2017*). However, there has been little consensus on signatures that will predict the course of disease in patients, possibly in part due to the heterogeneity of mechanisms that lead to active disease (*Nogueira et al., 2022*).

The murine model of TB infection is a useful tool for analysis of host immune responses to infection due to the abundance of available reagents, ability to precisely control experimental conditions, and ease of genetic manipulation. Importantly, the mouse model captures much of what is known about human immune responses to *Mtb*, including the importance of CD4 T cells and IFN-γ for immune control of infection (*Green et al., 2013*; *Caruso et al., 1999*; *Flynn et al., 1993*; *Scanga et al., 2000*; *Cooper et al., 1993*). However, current mouse models fail to recapitulate several aspects of *Mtb* infection, including spontaneous resolution of infection as well as the widely varying susceptibility and patterns of disease seen in humans. Although there are minor differences in susceptibility to infection, most commonly used mouse lines all exhibit similar infection dynamics and characteristics. However, despite the limited diversity of common laboratory lines, comparison of divergent phenotypes followed by genetic mapping has identified loci that contribute to susceptibility to mycobacterial infection, leading to valuable insights into immune factors that influence susceptibility to infection. An example is the characterization of the *Sst1* locus, which regulates type I IFN signaling through the gene *Sp140*, a repressor of type I IFN (*Ji et al., 2019*; *Pan et al., 2005*; *Kramnik et al., 2000*; *Kramnik et al., 1998*). Excessive production of type I IFN in *Sst1* susceptible (*Sst1ˢ*) mice, which have a loss of function mutation of *Sp140*, elicits increased IL-1 receptor antagonist (IL1-Ra) expression which competes with IL-1 for binding to the IL-1R. IL-1 is crucial for control of infection and the functional deficiency in IL-1 signaling in *Sst1ˢ* mice results in increased susceptibility to *Mtb* (*Ji et al., 2019*; *Ji et al., 2021*). Analysis of the phenotype of these highly susceptible mice led to the discovery of a mechanism by which type I IFN is detrimental to host infection. These studies suggest that increasing the genetic diversity in mouse models will lead to the discovery of additional genetic loci that are important for modulating the outcome of *Mtb* infection.

Historically, most *Mtb* infectious studies in the mouse model have been conducted using only a handful of lines: C57BL/6 (B6), BALB/C, and C3Heb/FeJ. In order to increase genetic diversity, new collections of mice have been established. The Collaborative Cross (CC) model was founded by crossing five common laboratory lines and three wild-derived lines (*Churchill et al., 2004*). Further breeding of the CC lines created the Diversity Outbred (DO) mouse collection, which is maintained as outbred population through random crossings. This is currently the most diverse mouse resource available (*Svenson et al., 2012*). Both cohorts have been used for the study of *Mtb* infection and display a range of disease phenotypes, including enhanced control or susceptibility to infection compared to standard laboratory lines (*Smith et al., 2016*; *Niazi et al., 2015*; *Gopal et al., 2013*). Infection of the DO cohort with *Mtb* revealed correlations between disease pathology and neutrophil influx, recapitulating features seen in human lung infections, in addition to identifying new inflammatory biomarkers that correlate with active human disease (*Niazi et al., 2015*; *Koyuncu et al., 2021*). Furthermore, these cohorts have been used to identify the genetic basis of disease responses. For example, the susceptibility of the CC042 line is associated with the loss of *Itgal* expression, an integrin required for T cell trafficking to the lung, resulting in decreased T cell trafficking and IFN-γ production in the lungs of infected animals (*Smith et al., 2019*).

Studies using CC and DO mice demonstrate the power of genetically diverse mice for identifying novel host regulators of immunity to *Mtb* (*Smith et al., 2022*). However, it is unclear whether these

collections capture the full spectrum of genetic diversity that exists in house mouse populations. To increase the genetic diversity of house mice available for the analysis of complex phenotypes, researchers recently created a set of 19 new inbred lines derived from wild mice collected across different geographic regions (*Phifer-Rixey et al., 2018*; *Moeller et al., 2018*; *Suzuki et al., 2020*). Unlike CC and DO mice, these new lines are all from the *Mus musculus domesticus* subspecies of house mouse. The use of a single subspecies to establish this cohort is beneficial, as it limits allelic conflicts that can arise from crossing different subspecies. This allows for the maintenance of natural genetic heterogeneity and makes the presence of genomic 'blind spots' – regions of the genome that are the same in all the lines – less likely (*Salcedo et al., 2007*; *Yang et al., 2011*). The mice that constitute this collection were originally collected across a latitudinal gradient from Brazil to Canada and show significant phenotypic diversity, including size, body mass index, and lipid and glucose metabolism (*Phifer-Rixey et al., 2018Phifer-Rixey et al., 2018*). Each line has been inbred through sib–sib mating for at least 10 generations, providing the benefit of the genetic reproducibility of laboratory-derived lines.

This new collection of wild-derived inbred lines represents a unique resource for identifying genetically diverse mice with enhanced or diminished susceptibility to *Mtb* infection and eventually, genes that control the host response to *Mtb* infection. Here we characterize 17 lines from this collection to identify lines that exhibit diminished control of *Mtb* infection at an early time point after infection (21 days) and analyze the accompanying immune responses. This is the first report of the use of this collection of mice for infectious disease or immunology-related phenotypes. Infection of the genetically diverse mouse lines reveals a range of responses with several lines showing higher susceptibility to infection compared with standard B6 mice. New susceptible lines of mice will be useful for identifying new mechanisms of susceptibility. In addition, we have identified heterogeneity in immune responses to infection that are distinct from known mouse lines, including robust control of infection in the absence of a strong Th1 T cell response and effective control of infection in the presence of elevated neutrophils. Our findings suggest that these mice will be useful not only for investigation of additional phenotypes in the context of TB infection but also may be useful for identifying novel immunological phenotypes more generally.

Results

Wild-derived mouse lines display variability in immune responses and susceptibility to *M. tuberculosis* infection

The cohort of wild-derived mice used in this study was established using outbred mice originally collected from five different localities across the Americas: Edmonton (EDM), Alberta, Canada; Saratoga Springs (SAR), New York, United States of America; Gainesville (GAI), Florida, United States of America; Tucson (TUC), Arizona, United States of America; and Manaus (MAN), Amazonas, Brazil (*Figure 1A*). Multiple individuals were trapped at each locale and used to create multiple, independent lines from an individual location. These mice exhibit a variety of phenotypic differences, including body weight, body length, body mass index (BMI), and glucose and lipid metabolism (*Phifer-Rixey et al., 2018*). Although there is within-group heterogeneity, separate lines of mice collected from a single location are in general more closely related genetically than mice collected from different locales (*Ferris et al., 2021*). We hypothesized that the genetic diversity of these mouse lines would contribute to heterogeneity in their capacity to control *Mtb* infection. We focused on a single time point, 21 days post-infection, to specifically identify early loss of control. Observing enhanced control of infection is also possible, though less likely to be observed at this relatively early time point after the onset of adaptive immunity. Mice were challenged with aerosolized *Mtb*, and the bacterial burden was assessed by colony-forming units (CFU) after 3 weeks of infection. CFU was normalized to inoculation dose day 1 post-infection to correct for any variability in inhaled bacterial load between mouse lines with different activity levels, sex, or different days of infection. The median bacterial burden varied over 100-fold between mice from different locales (*Figure 1B*). Surprisingly, individual mouse lines that originated from the same locale demonstrated a wide variation in susceptibility, suggesting that genetic heterogeneity within the closely related lines can influence the outcome of infection. Bacterial burdens in the lungs of mice from the MANC line are significantly higher compared to the closely related MANA, MANB, and MANE lines which are approximately as resistant as the standard
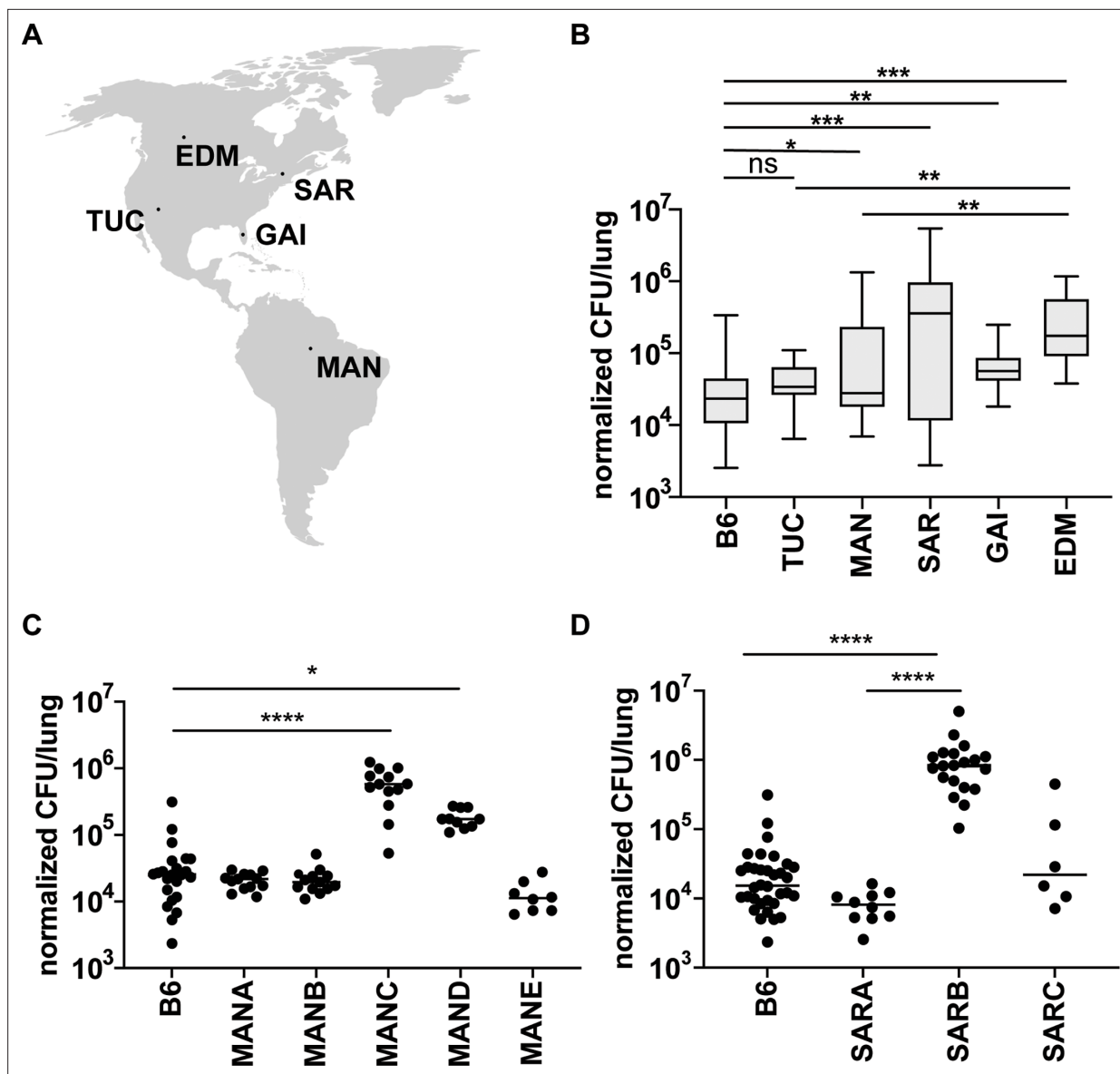
Figure 1. Mouse lines from different geographical regions show variable susceptibility to *Mtb* infection. (**A**) Mice were collected from five different sites across the Americas and inbred to generate individual genetic lines from each location. Map obtained from https://simplemaps.com/resources/svg-world. (**B**) Bacterial burden in the lungs of the mice derived from the different locations at 21 days post-infection with aerosolized *Mtb*. Comparison of the susceptibility among genetically distinct Manaus lines (**C**) or Saratoga lines (**D**) infected with aerosolized *Mtb*. The average inoculum dose is 400 CFU/mouse. CFU data was normalized to CFU enumeration on day 1 to correct for variation in inoculum dose between experimental days. EDM: Edmonton, SAR: Saratoga Springs, TUC: Tucson, GAI: Gainesville, MAN: Manaus. Data represent 2–6 independent experiments for each mouse line with 6–34 mice per line. Each dot represents a mouse. The p values were determined using a Kruskal–Wallis ANOVA. *$p < 0.05$, **$p < 0.01$, ***$p < 0.001$, ****$p < 0.0001$.

The online version of this article includes the following figure supplement(s) for figure 1:

Figure supplement 1. Variation in susceptibility to infection in wild mice does not depend on mouse weight or sex.

B6 (*Figure 1C*). Mice from the MAND line show an intermediate phenotype. We also observed significant variability in bacterial burdens in mice from Saratoga Springs. Whereas SARA and SARC mice are at least as resistant to infection as the standard B6, SARB lines harbor significantly more bacteria in the lungs at 3 weeks post-infection (*Figure 1D*). Smaller differences in susceptibility are found in the lines from Tucson, Gainesville, and Edmonton (*Figure 1—figure supplement 1A–C*).

A low BMI has been shown to be a risk factor for TB in humans (*Lönnroth et al., 2010*). Because the different lines of wild mice vary considerably in body weight even when provided the same diet,

we examined whether differences in body weight could account for differences in the ability to control infection. For this analysis, we focused on the Saratoga Springs and Manaus lines of mice where we observed the highest amount of variability in the control of infection. We found that there were significant differences in the starting weight of mice prior to infection when comparing the different lines, with a trend toward increased body weight in mice from Saratoga Springs (*Figure 1—figure supplement 1D*). However, we did not find a correlation between body weight and TB control in these well-nourished mice (*Figure 1—figure supplement 1E*). Similarly, previous reports have suggested that sex plays a role in susceptibility to infection, with females being more susceptible to TB infection in both mice and humans. We also observed no differences in bacterial burden at 21 days post-infection between male and female mice (*Figure 1—figure supplement 1F*). This is not surprising, as demonstrated differences in the ability of male and female mice to control infection emerged only at late time points ~200 days after infection (*Dibbern et al., 2017*).

We next reasoned that genetically determined differences in immune responses to infection might underlie the differences in susceptibility observed between different lines of wild-derived mice. To identify immune correlates of bacterial burden in the lungs of the infected wild mouse lines, we evaluated the presence of major immune cells thought to play a role in infection using flow cytometry in parallel with CFU counts at 21 days post-infection. We observed variability in the relative proportions of macrophages, neutrophils, CD4 T cells, CD8 T cells, and B cells when comparing individual lines (*Figure 2A–E*, *Figure 2—figure supplement 1*). Because the strains are very different in body size, in this case, proportion is more informative than absolute cell numbers. The most striking differences observed were in CD11b+Ly6G+ neutrophils, both when comparing individual lines isolated from a single geographic site and when comparing mice originally derived from different locales (*Figure 2A–E*).

In order to determine whether observed differences in the proportions of immune cells may drive the outcome of infection, we examined correlations between cell type and bacterial burden. We found significant correlations between the proportion of CD3+, CD4+, CD8+, and B220+ cells with control of infection, with larger proportions of these cells corresponding to lower CFU in the lung (*Figure 2F–I*, *Figure 2—figure supplement 2A*). In contrast, we found that the proportion of neutrophils in the lung could explain approximately 60% of the variation seen in the wild-derived mice, with higher neutrophil burden associated with higher CFU in the lungs (*Figure 2J*). This is consistent with numerous studies of susceptible mice on the B6 background that have pointed to a role for excessive infiltration of neutrophils in promoting lung pathology and susceptibility to *Mtb* infection (*Kimmey et al., 2015*; *Mishra et al., 2017*; *Nair et al., 2018*; *Dorhoi et al., 2010*). Production of IFN-γ by T cells is known to be important for control of infection (*Green et al., 2013*; *Cadena et al., 2016*; *Mogues et al., 2001*; *Bold and Ernst, 2012*). As expected, B6 mice exhibit a high proportion of IFN-γ producing CD4 T cells and lower bacterial burden in the lungs compared to several wild mice lines (*Figure 2K*). This was particularly evident in mice from Saratoga Springs (SAR). The SARA line controls bacterial CFU in the lungs in the presence of very few IFN-γ producing CD4 T cells (*Figure 2—figure supplement 2B*). No correlations were found between bacterial burden and the proportion of IFN-γ producing CD8 T cells or CD11b+ cells (*Figure 2L, M*). The overall variation in bacterial burden and immune cells present in the lung among and between the locales indicates the heterogeneity in underlying immune responses to *Mtb* infection. The notable differences between the wild-derived mouse lines and B6 mice show the potential for identifying novel mechanisms of susceptibility to infection in these mice.

Macrophages from Manaus lines show no intrinsic defects that correlate with control of infection

Despite being closely genetically related, the Manaus lines show distinct susceptibilities to *Mtb*. Whereas most of the tested lines control infection in the lungs as well as B6, the MANC line is significantly more susceptible to infection (*Figure 1C*). We therefore focused on these lines for a more in-depth immunological analysis. First, we tested whether impaired bacterial restriction in the MANC line can be explained by differences in cell intrinsic responses in host cells. Macrophages are central to *Mtb* infection, serving both as the host cell, the cell responsible for killing the bacteria, and an important source of cytokines that regulate infection (*Cohen et al., 2018*; *Srivastava et al., 2014*; *Domingo-Gonzalez et al., 2016*; *Ravesloot-Chávez et al., 2021*). To elucidate whether macrophage
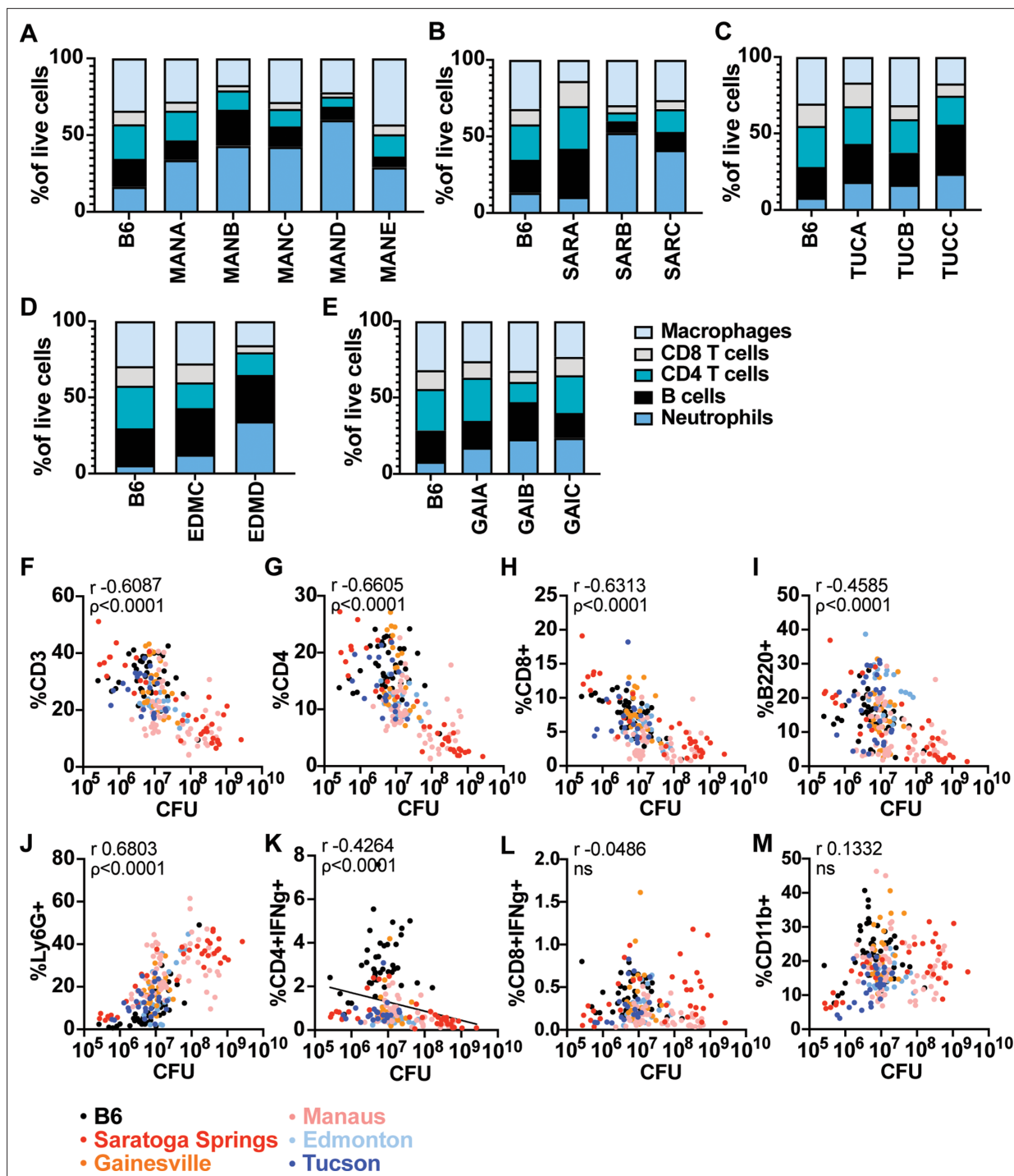
Figure 2. Genetic diversity translates into variability in bacterial burden and immune cells in the lung during *Mtb* infection. Cellular percentages were enumerated in the lungs using flow cytometry at 21 days post-infection with *Mtb* between and within mouse lines from different locales (**A–E**). The correlation between immune cell type (as shown in **A–E**) and CFU in the lung is depicted for individual mice (**F–M**). Data represent 2–6 independent experiments for each mouse line with 6–34 mice per line. The p value was determined using two-tailed Spearman correlations.

The online version of this article includes the following figure supplement(s) for figure 2:

Figure supplement 1. Cell percentages from flow cytometry-based analysis in the lungs of infected wild mice relative to B6.

Figure supplement 2. The proportion of IFN-γ producing CD4 T cells in the lung does not correlate with bacterial burden.

Figure supplement 3. Immune cell composition in the lungs of infected mice.
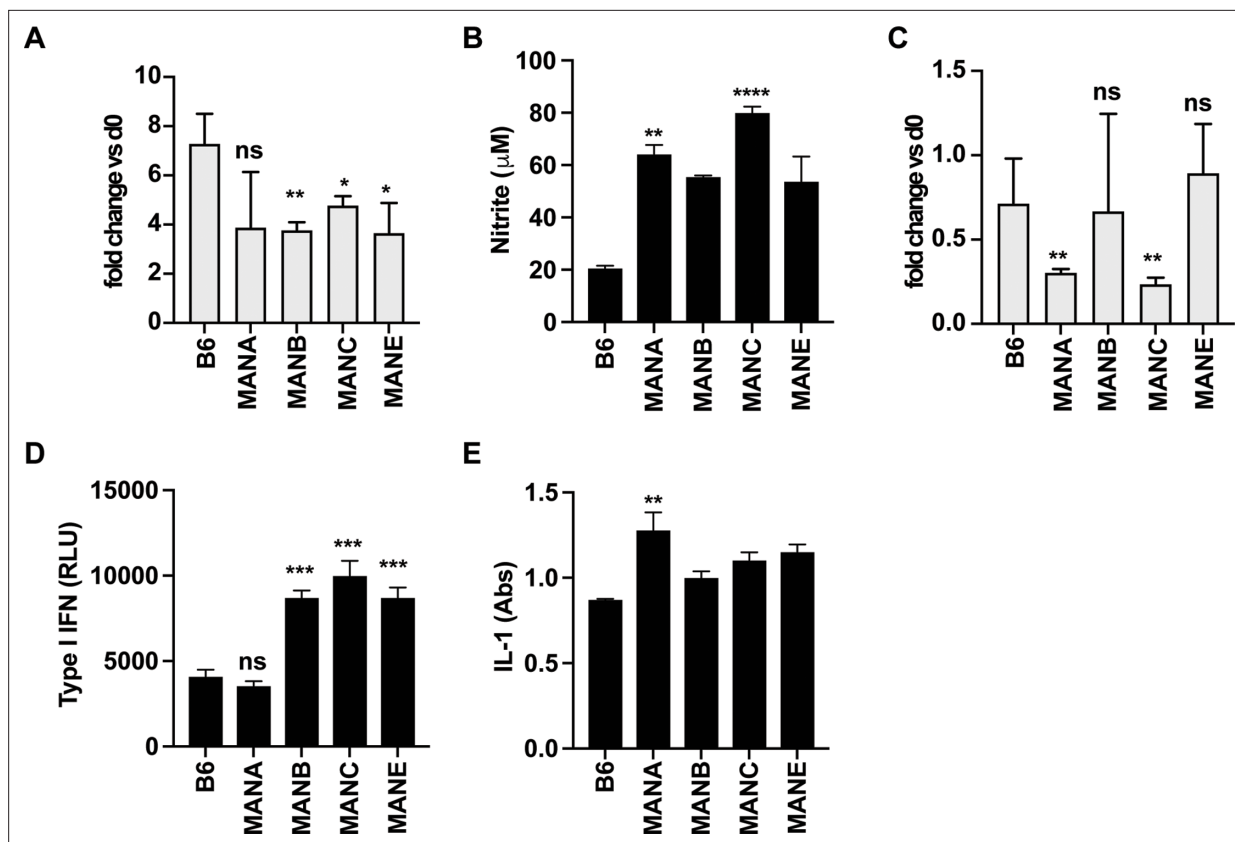
Figure 3. Intrinsic control of infection and response to IFN-γ is not impaired in macrophages from wild-derived mice. (**A**) Bone marrow-derived macrophages (BMDM) isolated from indicated mouse lines were infected with *Mtb* and bacterial growth was determined at 4 days post-infection by enumerating CFU. (**B**) The presence of nitrite in the supernatant was determined by Griess assay at 48 hr post-infection. (**C**) IFN-γ-activated BMDM were infected with *Mtb* and CFU were measured on day 4 post-infection. Production of type I IFN (**D**) or IL-1 (**E**) was measured at 24 hr post-infection with reporter cell lines. Data are representative of two independent experiments. The p values were determined using a Kruskal–Wallis ANOVA. *p < 0.05, **p < 0.01, ***p < 0.001 ****p < 0.0001.

responses differ between mouse lines, bone marrow-derived macrophages (BMDM) from four Manaus lines were prepared and infected with *Mtb* followed by quantification of bacterial burden and cytokine production. Macrophages from all the tested lines, including B6, allow the growth of *Mtb* in the absence of exogenous cytokine stimulation (*Figure 3A*), with none of the lines exhibiting a loss of control relative to B6. Indeed, we observed a slight decrease in bacterial replication in MANB, MANC, and MANE relative to B6 (*Figure 3A*). Additionally, all macrophages responded similarly to IFN-γ stimulation, producing significantly more nitric oxide (NO) upon infection than is observed with B6 (*Figure 3B*). Similarly, we did not observe any defects in IFN-γ-based control of infection at the macrophage level as all MAN lines controlled infection as well or better than the standard B6 (*Figure 3C*). Thus, differences in cell intrinsic control of infection that are evident ex vivo do not obviously play a role in the susceptibility of the MANC line to *Mtb* infection.

Type I IFN is known to be a major driver of susceptibility in mice, and possibly humans (*Ji et al., 2019*; *Dorhoi et al., 2014*; *Desvignes et al., 2012*; *Antonelli et al., 2010*; *Berry et al., 2010*; *Zak et al., 2016*; *Singhania et al., 2018*; *Scriba et al., 2017*; *Llibre et al., 2019*). Macrophages from *Sp140*⁻/⁻ mice that are highly susceptible to infection produce excessive type I IFN upon immune stimulation, recapitulating the high type I IFN/low IL-1 signaling phenotype of these animals in vivo. We next tested whether increased type I IFN or impaired IL-1 production by infected macrophages could underlie the high bacterial burden. Macrophages were infected with *Mtb* and levels of type I IFN were assessed at 24 hr post-infecting using interferon-stimulated response element (ISRE)-L929 reporter cells (*Jiang et al., 2005*). We found that macrophages isolated from three MAN lines (MANC, MANB, and MANE) produced significantly more type I IFN than B6 or MANA (*Figure 3D*); however, these

findings did not correlate with the ability to control infection in vivo (*Figure 1C*). We also measured IL-1 bioactivity in the supernatants of infected macrophages using the HEK-Blue IL-1R cell line and found that in vitro production of IL-1 was comparable to other Manaus genotypes and to B6. Taken together, unlike the majority of susceptible mouse lines, none of the Manaus lines appear to have major macrophage intrinsic defects observable that would explain the observed differences in control of infection in vivo.

Heterogeneity in neutrophil phenotypes drives differences in bacterial burden

Neutrophils possess potent antimicrobial mechanisms, yet their role in host defense during *Mtb* infection is not well defined. In human TB, neutrophils are generally associated with active disease and pathogenesis (*Gopal et al., 2013*; *Eum et al., 2010*; *Lowe et al., 2012*). The vast majority of mouse lines with excessive accumulation of neutrophils in the lung have high bacterial burdens in the lung and are susceptible to infection (*Niazi et al., 2015*; *Mishra et al., 2017*; *Nandi and Behar, 2011*; *Eruslanov et al., 2005*; *Lyadova et al., 2010*; *Marzo et al., 2014*; *Keller et al., 2006*). Interestingly, the majority of the Manaus lines show high neutrophilic influx to the lungs compared to B6 mice, despite the strong variability in bacterial burden (*Figures 1C and 2A*). In general, the proportion of neutrophils in the lung is a clear predictor of susceptibility to infection across all lines examined (*Figure 2J*, *r* = 0.6803). Indeed, we observed strong correlations in the proportion of neutrophils in the lungs with susceptibility to infection in B6 mice, which overall have robust control of infection (*Figure 2—figure supplement 3A*) as well as mice from Saratoga Springs, which encompass both susceptible and resistant lines (*Figure 2—figure supplement 3B*). However, when examining mice from Manaus, we found a significantly decreased correlation in the proportion of neutrophils in the lungs and the total CFU, in line with our initial observation that these mice tend to have a higher proportion of neutrophils in the lungs than B6 despite variability in CFU (*Figure 2—figure supplement 3C*). These data suggest that mice from Manaus may have phenotypic heterogeneity in neutrophil populations that results in diminished correlation between neutrophils and susceptibility to infection.

Recently, studies have suggested that neutrophils are functionally heterogeneous cells and can participate in the inflammatory response in both protective and deleterious roles. This prompted us to investigate the phenotypes of neutrophils in the Manaus lines during infection. We first sought to recapitulate our CFU and neutrophil data in experiments where we focused only on B6 and Manaus lines. Mice from Manaus controlled infection with *Mtb* as well as B6 mice, as measured by CFU in the lungs at 25 days post-infection, with the exception of the MANC line (*Figure 4A*). All Manaus mice have a higher proportion of neutrophils in the lungs (*Figure 4B*). In addition, when comparing the absolute number of neutrophils in the lungs of infected mice, MANB and MANC had elevated, roughly equivalent, absolute numbers of neutrophils in the lungs (*Figure 4C*), despite very different bacterial burdens (*Figure 4A*). We next tested whether the high neutrophilic influx in the lungs of MANC mice drives susceptibility to infection. We treated mice with an antibody targeting Ly6G to deplete neutrophils. Antibody depletion resulted in a dramatic drop of ~40-fold in CFU in the lungs of MANC mice (*Figure 4D, E*). In contrast, depleting neutrophils from B6 or MANB mice had a more modest effect on CFU burden of two- to threefold (*Figure 4F*). Thus, in MANC mice, neutrophils are an important driver of susceptibility.

Granuloma-like structures in MANC mice are dominated by neutrophils and have a paucity of both macrophages and T cells

Because both MANB and MANC mice have elevated levels of neutrophils in the lungs relative to B6, we next sought to determine whether the spatial localization of neutrophils differed between these lines. To do so, we used immunofluorescence microscopy to characterize granuloma-like structures in MANB and MANC mice infected with *Mtb*. Both MANB and MANC lesions contained large numbers of neutrophils as determined by staining with both CD11b and Ly6G antibody. Whereas neutrophils appeared as discrete cells within lesions of MANB mice (*Figure 4G*), neutrophils in MANC lesions appeared to form large aggregates of cells (*Figure 4H*). In addition, there was twice the amount of neutrophil staining per area in MANC lesions relative to MANB (*Figure 4I*) and far fewer CD4 T cells within MANC lesions than within MANB lesions (*Figure 4J*).
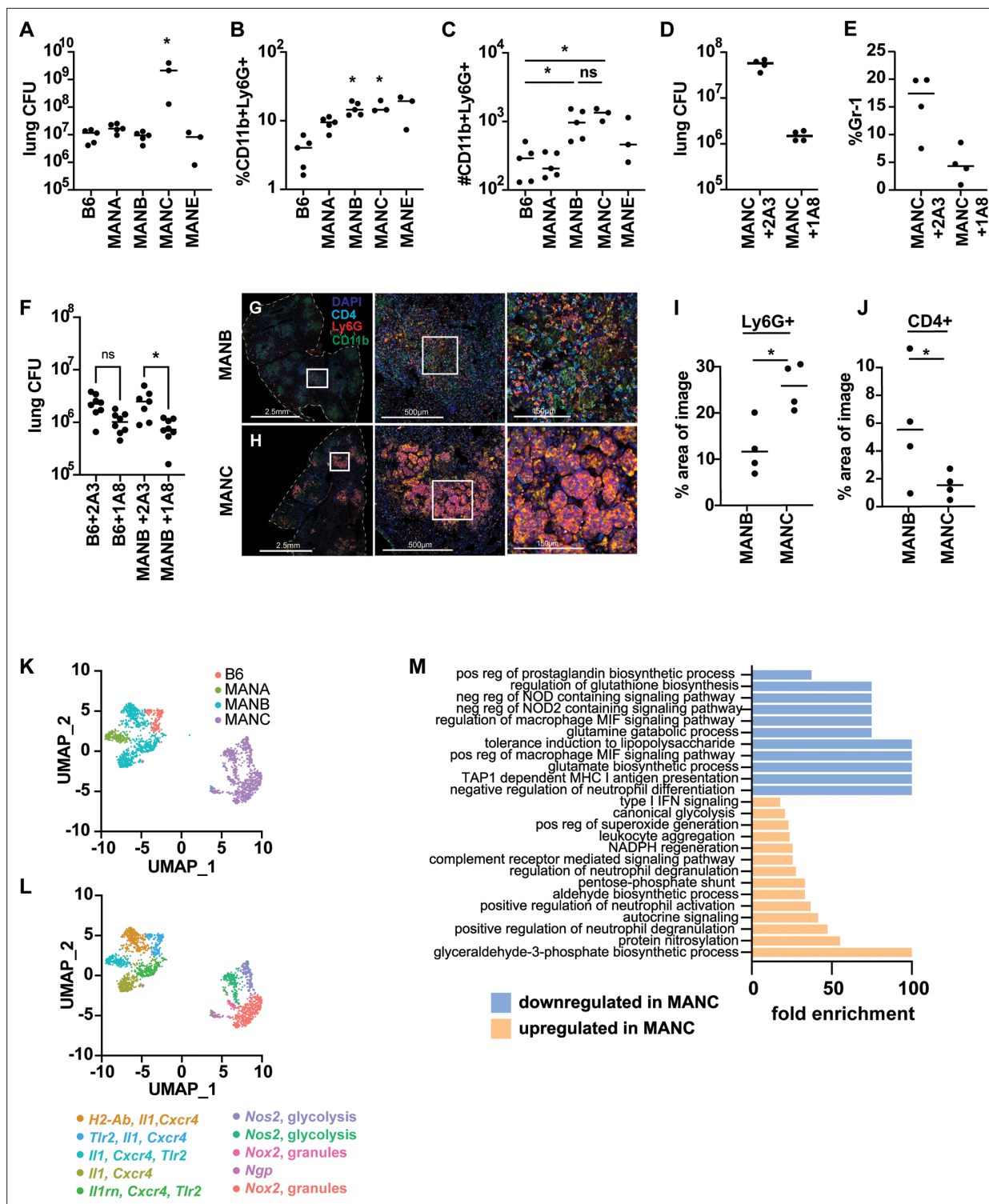
Figure 4. Diverse populations of neutrophils are present during infection of Manaus mice. (**A**) Bacterial burden in the lung was assessed in Manaus mice at 25 days post-infection. (**B, C**) Percentages and absolute counts of CD11b+Ly6G+ cells in the lungs at 25 days post-infection were enumerated by flow cytometry. Percentage is relative to the total number of live cells. (**D, E**) MANC and MANB (**F**) mice were treated with neutrophil-depleting antibody (1A8) or isotype control (2A3) every other day starting on day 11 post *Mtb* infection. Bacterial burden and neutrophil numbers were quantified on day 25 post-infection. Immunofluorescent microscopy on fixed lung tissues from MANB (**G**) and MANC (**H**) mice at 21 days post-infection. Area quantification of Ly6G+ (**I**) or CD4+ (**J**) staining in lung sections. (**K, L**) UMAP clustering of neutrophils from scRNAseq data of live cells in the lung at 21 days post *Mtb* infection. Signature functional genes that are characteristic of each cluster are provided with color coding according to cluster. (**M**) Gene

Figure 4 continued on next page

Figure 4 continued

ontology enrichment analysis of pathways down- or upregulated in MANC neutrophils compared with other neutrophil genotypes shows enrichment of genes involved in neutrophil activation and metabolism. CFU and antibody depletion data are representative of three independent (MANC) or two independent (MANB) experiments. The p values were determined using Mann–Whitney *U* test (**A, I, J**) and Kruskal–Wallis ANOVA (**B, C**), *p < 0.05. scRNAseq data represent a single experiment with pooled tissues from four mice.

The online version of this article includes the following figure supplement(s) for figure 4:

Figure supplement 1. Immune cell composition in the lungs of infected mice.

Figure supplement 2. T cell subsets and gene expression in wild-derived mice.

In order to elucidate the phenotypic differences of the cell populations in the different wild-derived mouse lines from Manaus, we used single-cell RNAseq (scRNAseq) to identify transcriptional changes in immune cells isolated from lungs of *Mtb*-infected B6, MANA, MANB, and MANC mice at 21 days post-infection. Using signature transcription factor, cytokine, and cell surface marker expression, the dataset was analyzed in the Seurat environment and major immune cell types in the lung were defined. Overall, transcriptional profiles indicated that the cell type composition was relatively similar across genotypes. The exception was an increase in cells identified as neutrophils (*Ly6g+*, *S100a8+*) in both MANB and MANC mice relative to the other genotypes, consistent with our flow cytometry data (*Figure 2—figure supplement 3D-G*).

To identify phenotypic heterogeneity within neutrophils, we subset neutrophils from all genotypes, identified variable features and rescaled the data within the subset, performed PCA dimension reduction and clustering, and visualized the results with the UMAP reduction. Neutrophils clustered into 2 major populations (*Figure 4K*) and at least 10 well-defined subpopulations (*Figure 4L*). B6, MANA, and MANB neutrophils clustered together while MANC neutrophils remained quite distinct. MANB neutrophils exhibited some transcriptional heterogeneity with two distinct neutrophil subpopulations distributed across two clusters (*Figure 4K*). B6 and MANA neutrophils were more homogeneous (*Figure 4K*). MANC clustered separately from neutrophils of any of the other genotypes and exhibited the most within-genotype heterogeneity in neutrophil subsets (*Figure 4K, L*). MANB and MANC mice exhibit comparably elevated numbers of neutrophils in their lungs during *Mtb* infection despite a 2-log difference in bacterial burden (*Figure 4A–C*). We next sought to further characterize transcriptional differences in MANC neutrophils relative to other genotypes across all neutrophil subtypes. Aggregated together, neutrophils from MANC mice were enriched for GO biological processes indicative of neutrophil activation, including positive regulation of neutrophil activation, neutrophil degranulation, superoxide generation, and glycolysis (*Figure 4M*). GO processes downregulated in MANC neutrophils relative to B6 included antigen processing, prostaglandin biosynthesis, and NOD signaling (*Figure 4M*). These data suggest that neutrophils from MANC mice are more activated and more likely to be engaging in processes that result in destruction of host tissue. To confirm these findings, and to determine if the gene expression signature identified to MANC mice is common to other mouse strains that have neutrophil-driven susceptibility to *Mtb*, we compared transcriptional signatures of neutrophils from our B6, MANB, and MANC datasets with transcriptional signatures of neutrophils isolated from *Sp140*^{−/−} mice. These mice have a type I IFN-driven susceptibility to infection that is also characterized by high levels of neutrophils. Depletion of neutrophils from this model rescues *Sp140*^{−/−} mice (*Kotov et al., 2023*). We used a series of recently developed signatures for neutrophil differentiation state (*Xie et al., 2020*) to generate scores for neutrophils across a number of parameters: neutrophil activation, NADPH oxidase, and secretory vesicles. In all cases, we found that MANC neutrophils scored higher across the parameters than any other genotype tested, including *Sp140*^{−/−} (*Figure 4—figure supplement 1*).

Neutrophils from MANC mice express higher levels of neutrophil signature genes, including *S100a8/9*, *Ngp*, and *Ly6g* (*Figure 5A*). These neutrophils also express higher levels of genes associated with pathogen clearance and host tissue damage, including inducible nitric oxide synthase (*Nos2*), NADPH oxidase (*Cybb*), and *Mmp9*. MANC neutrophils' glycolytic signature includes higher expression levels of *Ldha* and *Pfkfb3*. Indeed, our clustering of MANC neutrophils clustered into subsets that were in part driven by differential expression of these marker genes (*Figure 4K*). In contrast, neutrophils from MANA, MANB, and B6 mice expressed higher levels of specific immune-related genes relevant to defense against *Mtb* infection including *Tlr2*, *Il1b*, and MHC II isoforms (*H2-Ab1* and *H2-Eb*) (*Figure 5A*). Other genes that were highly differentially expressed between the lines
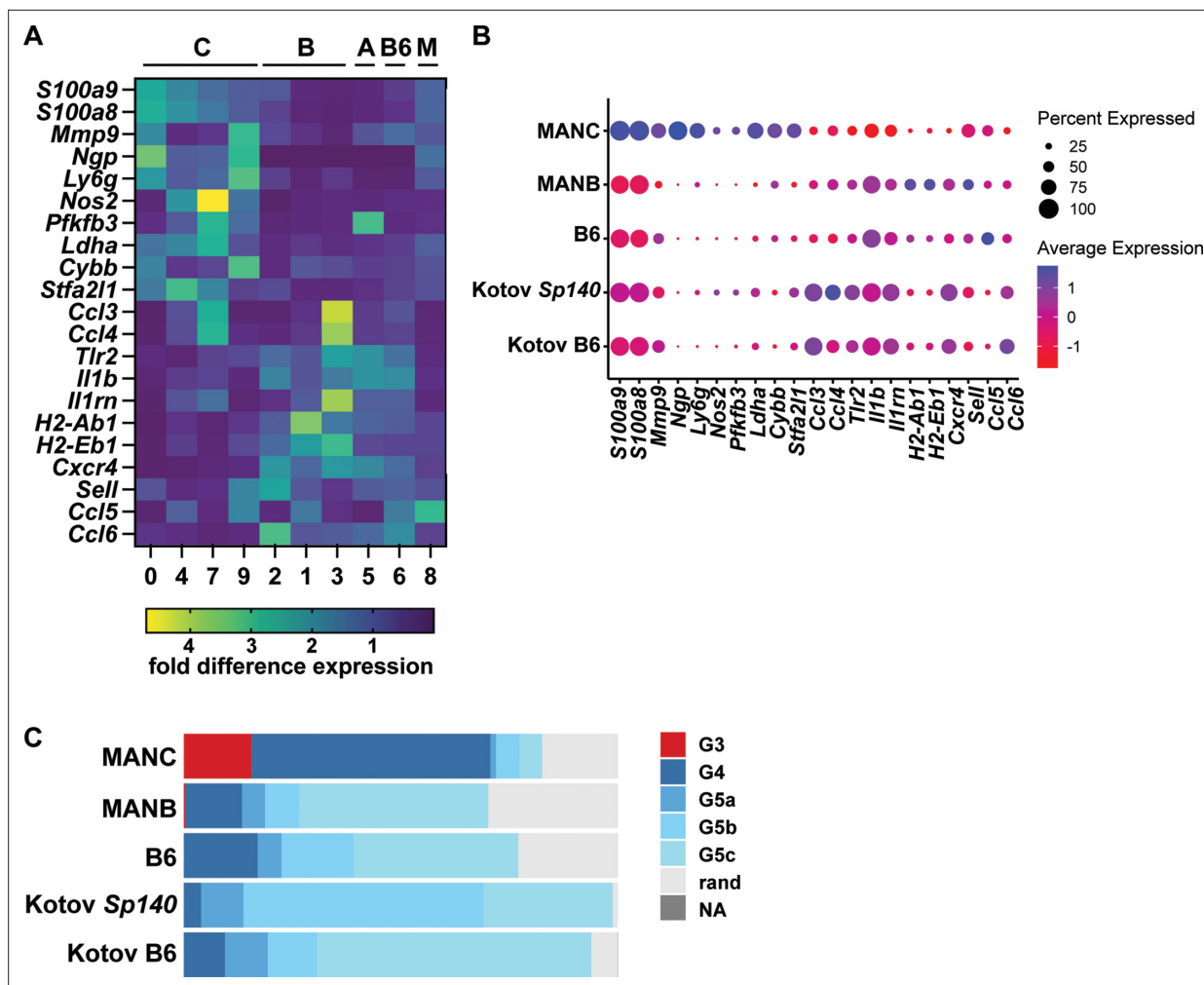
Figure 5. Neutrophil signature of MANC mice is unique relative to other susceptible mouse lines. (**A**) Comparison of gene expression between highly expressed genes in the MANC neutrophil clusters with expression in MANB (**B**), MANA (**A**), B6, and clusters of mixed genotype (M). (**B**) Comparison of MANC signature genes with expression of genes in the *Sp140*⁻/⁻ susceptible mouse line. (**C**) MANC neutrophil signature according to neutrophil developmental stage.

were the chemokines *Ccl3*, *Ccl4*, *Ccl5*, and *Ccl6* (**Figure 5A**). Neutrophils from all lines expressed very low levels of immunosuppressive proteins and cytokines, with the exception of IL-1R antagonist (*Il1rn*), which was highly expressed by a subset of MANB neutrophils (**Figure 5A**). In summary, neutrophils in susceptible MANC mice exhibit a transcriptional program that is unique when compared with other MAN lines or to B6 mice. We compared this signature with the transcriptional signature of *Sp140*⁻/⁻ and again found that the MANC transcriptional signature is unique to neutrophils from this line and not a common feature of high bacterial burden or neutrophil-driven pathology during *Mtb* infection (**Figure 5B**).

Premature release of neutrophils at early developmental stages is a hallmark of some inflammatory states, a phenomenon associated with emergency granulopoiesis (**Manz and Boettcher, 2014**). These immature neutrophils, also known as banded neutrophils, have been shown to exhibit a hyperactivated state. Using our scRNAseq data, we evaluated the differentiation state of neutrophils from B6 and Manaus mice and compared them with neutrophils from *Sp140*⁻/⁻ mice. Interestingly, we found that neutrophils from the lungs of Mtb-infected MANC mice were uniquely found to exhibit an immature transcriptional phenotype dominated by G3 (immature neutrophils) and G4 (mature neutrophils prior to release from bone marrow). All other genotypes were dominated by mature peripheral neutrophils G5a, G5b, and G5c cells, as expected (**Figure 5C**).

CD4 T cells from MANC mice are not significantly different from CD4 T cells from other lines

We showed that granuloma-like lesions from MANC mice exhibited a paucity of T cells (*Figure 4G–J*). These data suggest that macrophages in lesions from MANC mice may differentially recruit neutrophils versus T cells, and/or that T cells may have an intrinsic defect in homing to lesions in MANC mice. To identify transcriptional differences in CD4 T cells and macrophage/monocyte populations that distinguish the lines of mice, we turned to our scRNAseq data. After subsetting CD4 T cells from all genotypes, renormalizing gene counts, PCA dimension reduction clustering, and visualizing a UMAP reduction, we identified 13 clusters that correspond to clearly distinct CD4 differentiation states (*Figure 4—figure supplement 2A*). All genotypes possessed naïve CD4 T cells, Th1 differentiated T cells, Ki67+ proliferating T cells, and cytotoxic T cells expressing granzyme B and perforin (cytotoxic CD4, *Figure 4—figure supplement 2B*). B6 mice uniquely had a population of what appear to be terminally differentiated Th1 T cells that express KLRG1 and high levels of IFN-γ (*Figure 4—figure supplement 2B*). These cells have been previously identified as a non-protective T cell subset in B6 mice (*Sakai et al., 2014*; *Cyktor et al., 2013*; *Lindenstrøm et al., 2013*). It is interesting that none of the Manaus lines appear to have this subset of T cells, even in the susceptible MANC line. Other markers of T cell activation and differentiation, including *Cd44*, *Pdcd1*, *Tigit*, and *Cd69*, were not substantially different across mouse lines (*Figure 4—figure supplement 2B*), suggesting that major phenotypic differences in CD4 T cells themselves, separate from their propensity for trafficking into or surviving within the granuloma, do not underlie the susceptibility of MANC mice. We also did not observe major differences in chemokine or chemokine receptor expression of genes known to be required for T cell trafficking into the lung parenchyma or into granulomas.

CD11b+/Ly6g− macrophage/monocyte-like cells were also mapped using our scRNAseq data and were found to fall into 14 distinct clusters, many but not all of which were genotype specific (*Figure 6—figure supplement 1A-B*). As expected, alveolar macrophages were observed in every genotype of mouse (*Figure 6—figure supplement 1A, B*). No clear pattern in terms of distribution of cell types emerged from analysis of markers for macrophages (*Adgre1*), monocytes (*Cx3cr1*), and inflammatory monocytes (*Ly6c*) (*Figure 6A*), although B6 and MANA were dominated by monocytes whereas MANB and MANC mice had clear macrophage populations (*Figure 6—figure supplement 1A, B*). A population of cells with mixed macrophage and monocyte markers was found in every genotype (*Figure 6—figure supplement 1A, B*). Similar to what we previously observed in neutrophils, monocyte/macrophages from MANC mice had a higher propensity to express *Nos2* (*Figure 6A*). No other genes indicative of macrophage function, including *IL1b*, *Arg1*, *Tnf*, and *Cybb*, were differentially expressed across genotypes (*Figure 6A*). Interestingly, MANC macrophages also exhibited very high levels of expression of *S100a9* and *S100a8*, genes more typically associated with neutrophil function (*Figure 6A*).

Global transcriptional changes in MANC immune cells reveal expanded expression of neutrophil markers across multiple cell lineages

Both macrophages and neutrophils from MANC mice express higher levels of *S100a8* and *S100a9* than cells from other genotypes. To identify differentially expressed genes in MANC mice whose expression patterns are preserved across multiple cell types, we analyzed scRNAseq data. Interestingly, we found that expression of a small number of genes was dramatically increased in MANC mice, and that this signature was dominated by genes that are often thought to be relatively neutrophil specific, including *Ngp* (neutrophil granule protein), *S100a9*, *S100a8*, and *lcn2* (lipocalin 2) (*Figure 6B*). Higher expression of these genes was not solely driven by higher expression levels in neutrophils, as we observed increased expression of these genes across all cell types analyzed, which included major immune cell populations as well as epithelial cells and fibroblasts isolated from lungs (*Figure 6C*). To determine whether expression of highly neutrophil-specific proteins has been observed in other cell types, we examined expression of *Ngp* across cell types in the ImmGen database (*Heng and Painter, 2008*), which holds curated expression data defined by immunological cell type and state. As expected, we found that expression of *Ngp* was observed at highest levels in neutrophils, with dramatically lower levels of expression across other immune cell types (*Figure 6—figure supplement 1C*). Thus, expression of these neutrophil-specific genes across many cell types appears to be a unique feature of MANC mice.
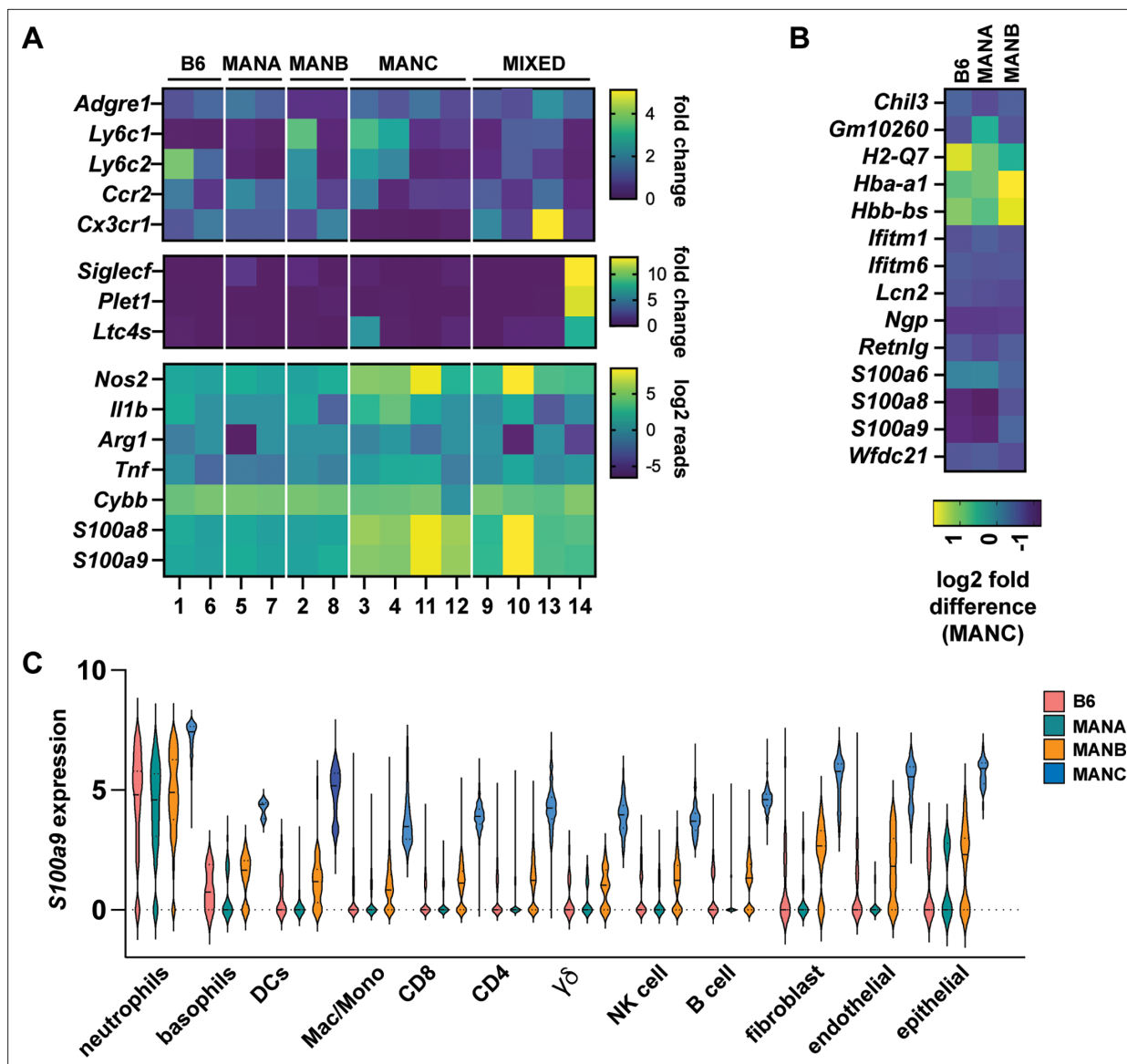
Figure 6. Expression of neutrophil markers across multiple cell lineages in MANC mice. (**A**) Heatmap of gene expression of markers of macrophage/monocyte subsets according to cluster and genotype. (**B**) Expression of indicated genes across all cell types comparing the B6, MANB, and MANC genotypes. (**C**) Violin plot of *S100a9* expression according to cell type and genotype.

The online version of this article includes the following figure supplement(s) for figure 6:

Figure supplement 1. Gene expression across immune cells.

Discussion

Developing immune-based diagnostics and new vaccines for TB has been challenging, likely due in part to the heterogeneity of human responses to disease. Host and bacterial genetics and environmental factors combine to shape the variety of disease outcomes seen in human TB. Furthermore, studies of human immune responses are by their nature rarely able to distinguish mechanisms that are causative of, rather than merely correlative with, disease outcomes. Thus, it has been difficult to answer some of the most important questions in the field. First, we lack an understanding of why some individuals experience a failure of immunity that results in progression to active disease. Further, reliable biomarkers of successful control of TB remain elusive, despite the importance of such biomarkers for guiding the development of new and effective vaccines. The strength of animal models comes from the ability to deeply interrogate novel immunological phenotypes and uncover unrecognized

mechanisms of infection control or susceptibility. Furthermore, the animal model can be used to establish causation based upon observations in humans. For example, there has been significant synergy between mouse and human immune studies for the establishment of type I IFN as an important driver of susceptibility to disease (*Berry et al., 2010*; *Stanley et al., 2007*; *Moreira-Teixeira et al., 2020b*; *Moreira-Teixeira et al., 2020a*). Identifying new immunological mechanisms in mice could lead to human studies focused on these mechanisms. Here we used a new collection of inbred wild mice to study the outcome of infection with *Mtb*. Wild mice exhibited a range in susceptibility at an early time point after infection as well as diversity in the immune responses to infection (*Figures 1 and 2*). Our initial survey of these mice has identified several lines with interesting and novel phenotypes worthy of in-depth investigation, including a unique neutrophil signature associated with susceptibility.

Neutrophils are thought to be an important driver of susceptibility to the outcome of TB in both mice and humans (*Mishra et al., 2017*; *Berry et al., 2010*; *Nandi and Behar, 2011*). It has been proposed that the neutrophils are detrimental to infection due to generation of lung inflammation and NETosis (*Moreira-Teixeira et al., 2020a*). It is still unclear what drives excess accumulation of neutrophils under different conditions. Further, neutrophils can adopt numerous phenotypes, and it is unclear whether all neutrophils are equally destructive during infection or whether specific neutrophil signatures are predictive of disease. Studying the role of neutrophils during *Mtb* infection has been challenging, due to the short lifespan and the subsequent difficulties of culturing neutrophils ex vivo. In addition, there are relatively few models of susceptibility to infection available for analysis. We found that neutrophils are highly abundant in the lungs of infected MANC mice, and that neutrophils drive the susceptibility of this line (*Figure 4A–E*). This finding accords with what has been shown by previous studies of other highly susceptible mice (*Kimmey et al., 2015*; *Mishra et al., 2017*; *Nair et al., 2018*; *Dorhoi et al., 2010*). However, MANB mice also harbor elevated levels of neutrophils, yet control infection as well as the standard B6 control. Histological data from the lungs of MANC mice show Ly6G staining for neutrophils reveals large aggregates of staining within the lesions of MANC mice, whereas neutrophils in MANB mice are more discrete and dispersed throughout the tissue (*Figure 4*). scRNAseq expression analysis shows that neutrophil clusters from MANC mice have a high expression of genes that contribute to neutrophil degranulation as well as superoxide and NO production, indicating potential for tissue destruction during infection. In addition, neutrophils from these mice exhibit a more activated glycolytic transcriptional signature when compared with B6 or other MAN lines. The transcriptional phenotype of protected MANB is strikingly different from MANC, with an expression profile that is associated with protective genes, including *Tlr2* and *Il1b*. We hypothesize that expression of these protective factors combined with a less activated phenotype means that MANB neutrophils may not drive pathology during Mtb infection. Whether these divergent phenotypes reflect differences in inherent immunological responses or are driven by underlying differences in the capacity of these mice to control infection will be an important topic for future study.

We found that neutrophils from highly susceptible MANC mice expressed high levels of *S100a8* and *S100a9* relative to other mouse lines, including the highly susceptible $Sp140^{-/-}$ line. *S100a8/a9* expression has been associated with numerous inflammatory states, including severe COVID-19 (*Udeh et al., 2021*; *Silvin et al., 2020*; *Boucher et al., 2024*). In addition, depletion of *S100a8* and *S100a9* was shown to improve chronic control of *Mtb* infection in mice (*Scott et al., 2020*). Finally, expression of these genes has been associated with progression of humans to active disease (*Scott et al., 2020*). Thus, MANC mice may represent an attractive model for studying the role of S100A8/A9 in TB as well as other inflammatory diseases. In addition to neutrophils, we observed increased expression of *S100a8* and *S100a9* (calprotectin) in macrophages and monocytes from MANC mice. Although typically used as a marker for neutrophils, due to high expression of these genes in this cell type, *S100a8* and *S100a9* are known to be expressed by other cell types including epithelial cells. Although it is technically possible that macrophages and monocytes in our dataset appear to express these markers because of phagocytosis of neutrophils, this is unlikely to explain high-level expression of these genes in other cell types.

Another intriguing aspect of the immune response to *Mtb* is the role of IFN-γ during infection. IFN-γ is mainly produced by CD4 T cells early during infection, and a lack of IFN-γ results in extreme susceptibility, with mice succumbing to infection (*Green et al., 2013*; *Flynn et al., 1993*). Furthermore, IFN-γ is required for prevention of bacterial dissemination to other tissues (*Sakai et al., 2016*). However, increased IFN-γ responses in the lung do not seem to correlate with resistance to infection

or improved responses to vaccination and can lead to exacerbated disease (*Tameris et al., 2013*; *Sakai et al., 2016*; *Leal et al., 2001*; *Majlessi et al., 2006*; *Mittrücker et al., 2007*). While local IFN-γ production might be necessary for full control of infection in B6 mice, additional research has shown effects of T cell-mediated IFN-γ independent mechanisms that contribute to control of infection, including through GM-CSF production by CD4 T cells (*Rothchild et al., 2014*; *Rothchild et al., 2017*; *Van Dis et al., 2022*) and the production of IL-17 (*Gallegos et al., 2011*). Several mouse lines in the cohort showed restriction of bacterial growth in the first weeks post-infection equally well but with widely differing IFN-γ+ T cell profiles. SARA mice exhibited enhanced control of bacterial burden (*Figure 1D*), but very low numbers of IFN-γ+ T cells compared to B6 mice (*Figure 2K*, *Figure 2—figure supplement 3*). This suggests either optimal localization of the few IFN-γ producing T cells to the bacterial-containing lesions, thereby allowing for highly efficient induction of local IFN-γ driven protective responses in the lesions, or the presence of IFN-γ or T cell-independent control of infection. Further research is needed to determine the spatial interactions between T cells and other immune cells present in the lesions, including bacilli-containing macrophages. It has previously been shown that homing of *Mtb*-specific T cells to the lung parenchyma is essential for interaction with activated macrophages to induce control of infection; however, signals that allow for T cell penetration into granulomas have not been fully elicited (*Sakai et al., 2016*). Finally, longitudinal studies are needed to determine whether control of infection in SARA mice persists over longer time periods.

The results presented here should inspire more in-depth mechanistic analysis of phenotypes observed in wild mouse lines by our group as well as others in the field. Ultimately, it will be important to identify genetic differences that underlie the differences in capacity to control disease. Inter-crossing of these closely related lines may elucidate genetic loci that are responsible for underlying phenotypes, possibly due to the presence of genetic variants that are absent in standard mouse lines. This strategy has been used with success by the breeding of susceptible C3H and resistant B6 mice to identify the super susceptibility locus 1 (*Sst1*) (*Kramnik et al., 2000*) as well as through the study of genetically diverse cohorts including the CC and DO mice which resulted in the identification of susceptibility markers (*Niazi et al., 2015*; *Smith et al., 2019*).

In addition to the abovementioned phenotypes, many other interesting correlates of immunity were identified in these mice that are worthy of future investigation. For example, we found a correlation between higher B cell numbers and improved resistance to infection; whether B cells may play a role in infection control is a question that can be examined using these lines. These and other phenotypes may be important not only for TB, but for other studies of host immunity. We suggest that these wild mice will be a rich source of phenotype discovery for numerous fields, adding to the heterogeneity of models available for the study of disease.

Materials and methods

Mice

Wild-derived mouse lines from the Manaus (MANA, MANB, MANC, MANE), Saratoga Springs (SARA, SARB, SARC), Edmonton (EDMA, EDMC, EDMD), Tucson (TUCA, TUCB, TACC), and Gainesville (GAIA, GAIB, GAIC) locations were obtained from the Nachman laboratory (UC, Berkeley). Several lines from these cohorts have since been deposited to The Jackson Laboratory (Bar Harbor, ME) as a public resource (ManA/NachJ #035354; ManB/NachJ #035355; ManE/NachJ #035365; SarA/NachJ #035346; SarB/NachJ #035347; SarC/NachJ #035348; TUCA/NachJ #035358; TUCB/NachJ #035359; GaiC/NachJ #035352). C57BL/6J (#000664) mice were obtained from The Jackson Laboratory and bred in-house. For mouse weight measurements, male mice were housed singly in a cage to avoid social dominance effects on weights. Female mice were group housed and body weights were measured at 7 weeks old and prior to infection with *Mtb*.

Bacterial culture

Low passage stocks of *Mtb* Erdman were grown in Middlebrook 7H9 liquid medium supplemented with 10% albumin-dextrose-saline or on solid 7H10 agar plates supplemented with 10% Middlebrook oleic acid, albumin, dextrose, and catalase (BD Biosciences) and 0.4% glycerol. Frozen stocks of *Mtb* were made from liquid cultures and used for all in vivo infection experiments.

In vivo infections

Mice were infected via the aerosol route with *Mtb* strain Erdman. Aerosol infection was done using a nebulizer and full-body inhalation exposure system (Glas-Col, Terre Haute, IN). Bacterial culture diluted in sterile water was loaded into the nebulizer calibrated to deliver ~400 bacteria per mouse, as measured by CFU in the lungs 1 day following infection (data not shown). Neutrophil depletion experiments were performed as described in *Nandi and Behar, 2011* using the anti-Ly6G monoclonal Ab (clone 1A8; BioXCell) or isotype control (clone 2A3, BioXCell). Two hundred micrograms of Ab were injected every other day starting at day 11 post-infection. Mice were sacrificed at 21 or 25 days post-infection to measure CFU and immune responses in the lungs. For bacterial enumeration, the largest lung lobe was homogenized in PBS supplemented with 0.05% Tween 80, and serial dilutions were plated on 7H10 plates. CFU were counted 21 days after plating. The three smallest lung lobes were harvested into complete RPMI (supplemented with 10% fetal bovine serum, 2 mM L-glutamine, 100 U/ml penicillin/streptomycin, 1 mM sodium pyruvate, 20 mM HEPES, 55 µM 2-mercaptoethanol), and strained through a 40-µm Falcon strainer. Cells were washed, stained with antibodies used for cytokine and surface marker staining: live/dead (L34970; Thermo Fisher Scientific), CD4, CD3, CD8a, CD11b, B220, Ly-6G (100509, 100219, 100707, 101237, 103233, 127627, respectively; BioLegend), and fixed/permeabilized with BD Cytofix/Cytoperm Fixation/Permeabilization Solution Kit (554714; Thermo Fisher Scientific) before staining with antibody specific for IFN-γ (505816; BioLegend). Data were collected using a BD LSR Fortessa flow cytometer and analyzed using FlowJo Software (Tree Star, Ashland, OR). All cell populations were gated on live cells. CD45 antibodies did not provide consistent staining for all wild mice genotypes. CD4 and CD8 cell populations were identified from CD3+ cells, followed by IFN-γ staining. Neutrophils were identified as CD11b+Ly6G+ and macrophages/monocytes as CD11b+Ly6G− (*Figure 2—figure supplement 2*).

IL-1 bioactivity reporter assay

The second largest lung lobe from infected mice was harvested into complete RPMI supplemented with Pierce proteinase inhibitor EDTA-free (Thermo Fisher Scientific), dissociated, and strained through a 40-µM Falcon strainer. Cells and debris were removed by a low-speed centrifugation (300 × *g*) followed by a high-speed centrifugation (2000 × *g*) and stored at –80°C. Samples were assayed using HEK-Blue IL-1R cells (InvivoGen, San Diego, CA). A total of 3.75×10^4 cells per well were plated in 96-well plates and allowed to adhere overnight in DMEM supplemented with 10% FBS, 2 mM L-glutamine. Reporter cells were treated overnight with 100 µl of sample (consisting of 50 µl of cell-free lung homogenates and 50 µl of media), or recombinant mouse IL-1β (R&D Systems 401-ML-005). Assays were developed using QUANTI-Blue (InvivoGen) according to the manufacturer's protocols and measured using a SpectraMax M2 microplate reader (Molecular Devices, San Jose, CA).

IFN-β bioactivity reporter assay

Interferon responsive ISRE-L929 cells (gift from D. Portnoy, UC Berkeley) were cultured in ISRE media (DMEM, 2 mM glutamine, 1 mM pyruvate, 10% heat inactivated FBS, and penicillin–streptomycin). The presence of type I interferon was assessed using lung homogenate as described above. Homogenates were applied in various dilutions to the interferon-responsive ISRE-L929 cells (5×10^4 cells/well) in white, 96-well, tissue culture-treated plates (Thermo Scientific Nunc). Cells were incubated for 4 hr, media aspirated, and cells were lysed with 30 µl Luciferase cell culture lysis reagent (Promega, Madison, WI). Finally, 100 µl of luciferase substrate solution (Promega) was added to each well and luminescence was measured using a Spectramax L luminometer (Molecular Devices).

QRT-PCR

The second largest lung lobe from infected mice was harvested into 500 µl RNAlater solution (Invitrogen Life Technologies, Carlsbad, CA) and stored at –80°C for qRT-PCR analysis. Tissues were transferred to 500 µl TRIzol (Invitrogen Life Technologies) and homogenized. Total RNA was extracted using chloroform, and the aqueous layer was further purified using RNeasy spin columns (QIAGEN, Hilden, Germany). For qPCR, cDNA was generated from 1 mg RNA using Superscript III (Invitrogen Life Technologies) and oligo(dT) primers. Select genes were analyzed using Power SYBR Green qPCR master mix (Thermo Scientific). Each sample was analyzed in triplicate on a CFX96 real-time PCR

detection system (Bio-Rad, Hercules, CA). CQ values were normalized to values obtained for GAPDH, and relative changes in gene expression were calculated as $\Delta\Delta C_Q$.

In vitro infections

Bone marrow was obtained from B6 and wild-derived mice and cultured in DMEM with 10% FBS, 2 mM L-glutamine, and 10% supernatant from 3T3-M-CSF cells for 6 days with feeding on day 3 to generate BMDM. BMDM were plated into 96- or 24-well plates with 5×10^4 and 3×10^5 macrophages/well, respectively, and were allowed to adhere and rest for 24 hr. BMDM were then treated with vehicle or recombinant mouse IFN-γ at 6.25 ng/ml (485-MI, R&D Systems) overnight and infected with *Mtb* Erdman strain at a multiplicity of infection of 5 in DMEM supplemented with 5% horse serum and 5% FBS, unless otherwise noted. After a 4-hr phagocytosis period, media was replaced with DMEM supplemented with 10% FBS, 2 mM glutamine, and 10% M-CSF. For IFN-γ-pretreated wells, IFN-γ was added post-infection at the same concentration. For enumeration of CFU, infected BMDM were washed with PBS and lysed in water containing 0.1% Triton X-100 for 10 min. Serial dilutions were prepared in PBS with 0.05% Tween 80 and were plated onto 7H10 plates. Supernatant nitrite was measured by Griess assay as a proxy for NO production by mixing supernatant 1:1 with a solution of 0.1% napthylethylenediamine, 1% sulfanilamide, and 2% phosphoric acid and measuring absorbance at 546 nm with a SpectraMax M2 microplate reader (Molecular Devices). Not every mouse line is included in in vitro profiling due to small litters and lack of availability of mice.

Immunofluorescent microscopy

Lung tissues were fixed in 10% neutral-buffered formalin at room temperature for 24 hr. Tissue embedding and sectioning at 5 μM was performed by the Center for Genomic Pathology Laboratory (UC Davis) and staining for anti-CD4 (D7D2Z, Cell Signaling Technology, Danvers, MA), anti-CD11b (M1/70, BioLegend), and anti-Ly6G (1A8, BioLegend) were performed by NanoString Technologies (Seattle, WA). Analysis of images for quantification was performed using ImageJ. Images were quantified at ×100 magnification.

scRNAseq and transcriptional analysis

The second largest lung lobes were pooled from five infected mice, tissue dissociated in RPMI 1640 containing liberase and DNase I in gentleMACS C tubes using the gentleMACS dissociator, strained through a 70-μM Falcon cell strainer in RPMI 1640 and counted. A total of 10,000 cells per sample were used for scRNAseq according to the 10x Genomics protocol. Briefly, single-cell suspensions were partitioned into Gel Beads in emulsion using the Chromium Next GEM Single Cell v3.1 system. Barcoded primers were used to reverse-transcribe poly-adenylated mRNA to produce barcoded, full-length cDNA. Purified DNA was amplified, fragmented, and amplified again to attach Illumina adapter sequences by the Functional Genomics Laboratory at UC, Berkeley. Libraries were sequenced on an Illumina NovaSeq S1 demultiplexed by the Vincent J. Coates Genomics Sequencing Laboratory at UC, Berkeley. Reads were aligned to the mouse transcriptome mm10 with the 10x Cell Ranger analysis pipeline using the Savio computational cluster at UC, Berkeley. Data can be found under GSE242343. After filtering, barcode counting, and unique molecular identifier counting, the Seurat 4.0.6 toolkit (Satija lab; *Hao et al., 2021*) was used to preprocess the data. Dimension reduction (PCA) and κ-nearest neighbor graph construction (25 PCs) was followed by clustering (resolution 0.75) and visualization of the data with UMAP reduction. The clustered data were manually assigned a cell type using signature genes and gene expression and visualization was explored using Seurat (*Supplementary file 1*). GO terms were analyzed using the top 200 differentially expressed genes of each dataset. For neutrophil and macrophage/monocyte analysis, the relevant cells were subset, variable features were re-identified, and the data rescaled within the subset. Dimension reduction (PCA) and κ-nearest neighbor graph construction (first 25 PCs), clustering (resolution 0.75) was followed by visualization and data exploration with the UMAP reduction. Differential gene expression was performed with Seurat's FindMarkers function. Gene ontology analysis was performed with topGO (v 2.48.0). The baseline of expression of neutrophil-related genes in mouse immune cell types (*Figure 6—figure supplement 1*) was obtained from the Immunological Genome Project MyGeneset application (http://rstats.immgen.org/MyGeneSet_New/index.html) using the ImmGen ULI RNA-seq dataset.

Neutrophil staging

Neutrophils were staged using single-cell transcriptional signatures developed by *Xie et al., 2020* (GSE137539) and a classifier constructed following methods developed by *Kim et al., 2022* using singleCellNet v. 0101 (*Tan and Cahan, 2019*). The classifier was trained with the scn_train() function and *nTopGenes* = 100, *nTopGenePairs* = 50, *nRand* = 50, *nTrees* = 1000. For comparison with wild mice neutrophils, B6 and Sp140$^{-/-}$ neutrophils were integrated from *Kotov et al., 2023* (GSE216023). Neutrophils from our dataset and Kotov's were subset into one unique Seurat object for each genotype and dataset. Integration anchors were found with *FindIntegrationAnchors()* followed by *IntegrateData()*. The combined, integrated dataset was then scaled, normalized, clustered, and inspected following dimensionality reduction with PCA and UMAP. The singleCellNet functions *sc_predict()* and *get_cate()* were used to classify cells in our dataset and to assign a neutrophil stage to each cell. Code for construction of Xie's neutrophil staging classifier, integration of the neutrophil datasets, and the assignment of neutrophil stages is available at GitHub (https://github.com/dmfox244/wm_neut_staging copy archived at *Fox, 2024*).

Statistical analysis

Data are presented as mean values, and error bars represent SD. Symbols represent individual animals. The statistical tests used are denoted in the legend of the corresponding figure for each experiment. Analysis of statistical significance was performed using GraphPad Prism 8 (GraphPad, La Jolla, CA), and p <0.05 was considered significant.

Additional information

Competing interests

Russell E Vance: R.E.V. is on the scientific advisory boards of Tempest Therapeutics and X-biotix. Sarah A Stanley: Sarah Stanley is on the scientific advisory board of X-biotix Therapeutics. The other authors declare that no competing interests exist.

Funding

Author contributions

Marietta M Ravesloot-Chavez, Conceptualization, Data curation, Formal analysis, Validation, Investigation, Visualization, Methodology; Erik Van Dis, Andrea Anaya-Sanchez, Investigation, Writing - review and editing; Douglas Fox, Data curation, Formal analysis, Investigation, Writing - review and editing; Scott Espich, Xammy Huu Nguyenla, Sagar Rawal, Helia Samani, Investigation; Mallory Ballinger, Henry F Thomas, Resources; Dmitri I Kotov, Formal analysis; Russell E Vance, Formal analysis, Supervision; Michael W Nachman, Conceptualization, Resources, Supervision, Writing - review and editing; Sarah A Stanley, Conceptualization, Data curation, Formal analysis, Supervision, Funding acquisition, Methodology, Writing - original draft, Project administration, Writing - review and editing

Author ORCIDs

Marietta M Ravesloot-Chavez ⓘ http://orcid.org/0000-0001-5129-7156
Xammy Huu Nguyenla ⓘ https://orcid.org/0000-0002-7532-8356
Dmitri I Kotov ⓘ https://orcid.org/0000-0001-7843-1503
Russell E Vance ⓘ https://orcid.org/0000-0002-6686-3912
Sarah A Stanley ⓘ https://orcid.org/0000-0002-4182-9048

Ethics

All procedures involving the use of mice were approved by the University of California (UC), Berkeley, Institutional Animal Care and Use Committee (AUP-2015-09-7979-2). All protocols conform to federal regulations and the National Research Council's Guide for the Care and Use of Laboratory Animals.

Peer review material

Reviewer #1 (Public review): https://doi.org/10.7554/eLife.102441.2.sa1
Reviewer #2 (Public review): https://doi.org/10.7554/eLife.102441.2.sa2
Author response https://doi.org/10.7554/eLife.102441.2.sa3

Additional files

Supplementary files

Supplementary file 1. Cellular expression markers used for scRNAseq cluster assignment following unbiased clustering.

MDAR checklist

Data availability

ScRNAseq data has been deposited in GEO, GSE242343.

The following dataset was generated:

Author(s)	Year	Dataset title	Dataset URL	Database and Identifier
Stanley AS, Ravesloot-Chavez MM	2025	Gene expression profile at single cell level on cells from the lungs of mice infected with Mycobacterium tuberculosis	https://www.ncbi.nlm.nih.gov/geo/query/acc.cgi?acc=GSE242343	NCBI Gene Expression Omnibus, GSE242343

References

Antonelli LRV, Gigliotti Rothfuchs A, Gonçalves R, Roffê E, Cheever AW, Bafica A, Salazar AM, Feng CG, Sher A. 2010. Intranasal Poly-IC treatment exacerbates tuberculosis in mice through the pulmonary recruitment of a pathogen-permissive monocyte/macrophage population. *The Journal of Clinical Investigation* **120**:1674–1682. DOI: https://doi.org/10.1172/JCI40817, PMID: 20389020

Berry MPR, Graham CM, McNab FW, Xu Z, Bloch SAA, Oni T, Wilkinson KA, Banchereau R, Skinner J, Wilkinson RJ, Quinn C, Blankenship D, Dhawan R, Cush JJ, Mejias A, Ramilo O, Kon OM, Pascual V,

Banchereau J, Chaussabel D, et al. 2010. An interferon-inducible neutrophil-driven blood transcriptional signature in human tuberculosis. *Nature* **466**:973–977. DOI: https://doi.org/10.1038/nature09247, PMID: 20725040

Bold TD, Ernst JD. 2012. CD4+ T cell-dependent IFN-γ production by CD8+ effector T cells in *Mycobacterium tuberculosis* infection. *Journal of Immunology* **189**:2530–2536. DOI: https://doi.org/10.4049/jimmunol. 1200994, PMID: 22837486

Boucher J, Gilbert C, Bose S, Tessier PA. 2024. S100A9: The unusual suspect connecting viral infection and inflammation. *The Journal of Immunology* **212**:1523–1529. DOI: https://doi.org/10.4049/jimmunol.2300640, PMID: 38709994

Cadena AM, Flynn JL, Fortune SM. 2016. The importance of first impressions: early events in *Mycobacterium tuberculosis* infection influence outcome. *mBio* **7**:e00342-16. DOI: https://doi.org/10.1128/mBio.00342-16, PMID: 27048801

Cadena AM, Fortune SM, Flynn JL. 2017. Heterogeneity in tuberculosis. *Nature Reviews. Immunology* **17**:691–702. DOI: https://doi.org/10.1038/nri.2017.69, PMID: 28736436

Caruso AM, Serbina N, Klein E, Triebold K, Bloom BR, Flynn JL. 1999. Mice deficient in CD4 T cells have only transiently diminished levels of IFN-gamma, yet succumb to tuberculosis. *Journal of Immunology* **162**:5407–5416 PMID: 10228018.

Churchill GA, Airey DC, Allayee H, Angel JM, Attie AD, Beatty J, Beavis WD, Belknap JK, Bennett B, Berrettini W, Bleich A, Bogue M, Broman KW, Buck KJ, Buckler E, Burmeister M, Chesler EJ, Cheverud JM, Clapcote S, Cook MN, et al. 2004. The Collaborative Cross, a community resource for the genetic analysis of complex traits. *Nature Genetics* **36**:1133–1137. DOI: https://doi.org/10.1038/ng1104-1133, PMID: 15514660

Cohen SB, Gern BH, Delahaye JL, Adams KN, Plumlee CR, Winkler JK, Sherman DR, Gerner MY, Urdahl KB. 2018. Alveolar macrophages provide an early *Mycobacterium tuberculosis* niche and initiate dissemination. *Cell Host & Microbe* **24**:439–446. DOI: https://doi.org/10.1016/j.chom.2018.08.001

Cooper AM, Dalton DK, Stewart TA, Griffin JP, Russell DG, Orme IM. 1993. Disseminated tuberculosis in interferon gamma gene-disrupted mice. *The Journal of Experimental Medicine* **178**:2243–2247. DOI: https://doi.org/10.1084/jem.178.6.2243, PMID: 8245795

Cyktor JC, Carruthers B, Stromberg P, Flaño E, Pircher H, Turner J. 2013. Killer cell lectin-like receptor G1 deficiency significantly enhances survival after *Mycobacterium tuberculosis* infection. *Infection and Immunity* **81**:1090–1099. DOI: https://doi.org/10.1128/IAI.01199-12, PMID: 23340310

Desvignes L, Wolf AJ, Ernst JD. 2012. Dynamic roles of type I and type II IFNs in early infection with *Mycobacterium tuberculosis*. *Journal of Immunology* **188**:6205–6215. DOI: https://doi.org/10.4049/jimmunol. 1200255, PMID: 22566567

Dibbern J, Eggers L, Schneider BE. 2017. Sex differences in the C57BL/6 model of *Mycobacterium tuberculosis* infection. *Scientific Reports* **7**:10957. DOI: https://doi.org/10.1038/s41598-017-11438-z, PMID: 28887521

Domingo-Gonzalez R, Prince O, Cooper A, Khader SA. 2016. Cytokines and chemokines in *Mycobacterium tuberculosis* infection. *Microbiology Spectrum* **4**:18-2016. DOI: https://doi.org/10.1128/microbiolspec. TBTB2-0018-2016, PMID: 27763255

Donovan ML, Schultz TE, Duke TJ, Blumenthal A. 2017. Type I interferons in the pathogenesis of tuberculosis: molecular drivers and immunological consequences. *Frontiers in Immunology* **8**:1633. DOI: https://doi.org/10. 3389/fimmu.2017.01633, PMID: 29230217

Dorhoi A, Desel C, Yeremeev V, Pradl L, Brinkmann V, Mollenkopf H-J, Hanke K, Gross O, Ruland J, Kaufmann SHE. 2010. The adaptor molecule CARD9 is essential for tuberculosis control. *The Journal of Experimental Medicine* **207**:777–792. DOI: https://doi.org/10.1084/jem.20090067, PMID: 20351059

Dorhoi A, Yeremeev V, Nouailles G, Weiner J, Jörg S, Heinemann E, Oberbeck-Müller D, Knaul JK, Vogelzang A, Reece ST, Hahnke K, Mollenkopf HJ, Brinkmann V, Kaufmann SHE. 2014. Type I IFN signaling triggers immunopathology in tuberculosis-susceptible mice by modulating lung phagocyte dynamics. *European Journal of Immunology* **44**:2380–2393. DOI: https://doi.org/10.1002/eji.201344219, PMID: 24782112

Eruslanov EB, Lyadova IV, Kondratieva TK, Majorov KB, Scheglov IV, Orlova MO, Apt AS. 2005. Neutrophil responses to *Mycobacterium tuberculosis* infection in genetically susceptible and resistant mice. *Infection and Immunity* **73**:1744–1753. DOI: https://doi.org/10.1128/IAI.73.3.1744-1753.2005, PMID: 15731075

Eum SY, Kong JH, Hong MS, Lee YJ, Kim JH, Hwang SH, Cho SN, Via LE, Barry CE III. 2010. Neutrophils are the predominant infected phagocytic cells in the airways of patients with active pulmonary TB. *Chest* **137**:122–128. DOI: https://doi.org/10.1378/chest.09-0903, PMID: 19749004

Ferris KG, Chavez AS, Suzuki TA, Beckman EJ, Phifer-Rixey M, Bi K, Nachman MW. 2021. The genomics of rapid climatic adaptation and parallel evolution in North American house mice. *PLOS Genetics* **17**:e1009495. DOI: https://doi.org/10.1371/journal.pgen.1009495, PMID: 33914747

Flynn JL, Chan J, Triebold KJ, Dalton DK, Stewart TA, Bloom BR. 1993. An essential role for interferon gamma in resistance to *Mycobacterium tuberculosis* infection. *The Journal of Experimental Medicine* **178**:2249–2254. DOI: https://doi.org/10.1084/jem.178.6.2249, PMID: 7504064

FoxD. 2024. Wm_neut_staging. swh:1:rev:aa34388f2ce599d78576e91198cc0f0adb5dff72. Software Heritage. https://archive.softwareheritage.org/swh:1:dir:099df4500d06c4177d415334b03f9625801ac07e;origin=https:// github.com/dmfox244/wm_neut_staging;visit=swh:1:snp:03a332c59cd7bf81429c44d3e856945ccb5cb3fa; anchor=swh:1:rev:aa34388f2ce599d78576e91198cc0f0adb5dff72

Gallegos AM, van Heijst JWJ, Samstein M, Su X, Pamer EG, Glickman MS. 2011. A gamma interferon independent mechanism of CD4 T cell mediated control of *M. tuberculosis* infection in vivo. *PLOS Pathogens* **7**:e1002052. DOI: https://doi.org/10.1371/journal.ppat.1002052, PMID: 21625591

Gopal R, Monin L, Torres D, Slight S, Mehra S, McKenna KC, Fallert Junecko BA, Reinhart TA, Kolls J, Báez-Saldaña R, Cruz-Lagunas A, Rodríguez-Reyna TS, Kumar NP, Tessier P, Roth J, Selman M, Becerril-Villanueva E, Baquera-Heredia J, Cumming B, Kasprowicz VO, et al. 2013. S100A8/A9 proteins mediate neutrophilic inflammation and lung pathology during tuberculosis. *American Journal of Respiratory and Critical Care Medicine* **188**:1137–1146. DOI: https://doi.org/10.1164/rccm.201304-0803OC, PMID: 24047412

Green AM, Difazio R, Flynn JL. 2013. IFN-γ from CD4 T cells is essential for host survival and enhances CD8 T cell function during *Mycobacterium tuberculosis* infection. *Journal of Immunology* **190**:270–277. DOI: https://doi.org/10.4049/jimmunol.1200061, PMID: 23233724

Hao Y, Hao S, Andersen-Nissen E, Mauck WM, Zheng S, Butler A, Lee MJ, Wilk AJ, Darby C, Zager M, Hoffman P, Stoeckius M, Papalexi E, Mimitou EP, Jain J, Srivastava A, Stuart T, Fleming LM, Yeung B, Rogers AJ, et al. 2021. Integrated analysis of multimodal single-cell data. *Cell* **184**:3573–3587. DOI: https://doi.org/10.1016/j.cell.2021.04.048, PMID: 34062119

Heng TSP, Painter MW. 2008. Immunological genome project consortium: networks of gene expression in immune cells. *Nature Immunology* **9**:1091–1094. DOI: https://doi.org/10.1038/ni1008-1091

Ji DX, Yamashiro LH, Chen KJ, Mukaida N, Kramnik I, Darwin KH, Vance RE. 2019. Type I interferon-driven susceptibility to *Mycobacterium tuberculosis* is mediated by IL-1Ra. *Nature Microbiology* **4**:2128–2135. DOI: https://doi.org/10.1038/s41564-019-0578-3, PMID: 31611644

Ji DX, Witt KC, Kotov DI, Margolis SR, Louie A, Chevée V, Chen KJ, Gaidt MM, Dhaliwal HS, Lee AY, Nishimura SL, Zamboni DS, Kramnik I, Portnoy DA, Darwin KH, Vance RE. 2021. Role of the transcriptional regulator SP140 in resistance to bacterial infections via repression of type I interferons. *eLife* **10**:e67290. DOI: https://doi.org/10.7554/eLife.67290, PMID: 34151776

Jiang Z, Georgel P, Du X, Shamel L, Sovath S, Mudd S, Huber M, Kalis C, Keck S, Galanos C, Freudenberg M, Beutler B. 2005. CD14 is required for MyD88-independent LPS signaling. *Nature Immunology* **6**:565–570. DOI: https://doi.org/10.1038/ni1207, PMID: 15895089

Keller C, Hoffmann R, Lang R, Brandau S, Hermann C, Ehlers S. 2006. Genetically determined susceptibility to tuberculosis in mice causally involves accelerated and enhanced recruitment of granulocytes. *Infection and Immunity* **74**:4295–4309. DOI: https://doi.org/10.1128/IAI.00057-06, PMID: 16790804

Kim M, Lu RJ, Benayoun BA. 2022. Single-cell RNA-seq of primary bone marrow neutrophils from female and male adult mice. *Scientific Data* **9**:442. DOI: https://doi.org/10.1038/s41597-022-01544-7, PMID: 35871169

Kimmey JM, Huynh JP, Weiss LA, Park S, Kambal A, Debnath J, Virgin HW, Stallings CL. 2015. Unique role for ATG5 in neutrophil-mediated immunopathology during *M. tuberculosis* infection. *Nature* **528**:565–569. DOI: https://doi.org/10.1038/nature16451, PMID: 26649827

Kotov DI, Lee OV, Fattinger SA, Langner CA, Guillen JV, Peters JM, Moon A, Burd EM, Witt KC, Stetson DB, Jaye DL, Bryson BD, Vance RE. 2023. Early cellular mechanisms of type I interferon-driven susceptibility to tuberculosis. *Cell* **186**:5536–5553. DOI: https://doi.org/10.1016/j.cell.2023.11.002, PMID: 38029747

Koyuncu D, Niazi MKK, Tavolara T, Abeijon C, Ginese M, Liao Y, Mark C, Gower AC, Gatti DM, Kramnik I, Gurcan M, Yener B, Beamer G. 2021. Tuberculosis biomarkers discovered using diversity outbred mice. *medRxiv*. DOI: https://doi.org/10.1101/2021.01.08.20249024

Kramnik I, Demant P, Bloom BB. 1998. Susceptibility to tuberculosis as a complex genetic trait: analysis using recombinant congenic strains of mice. Novartis Foundation Symposium. 120–131. DOI: https://doi.org/10.1002/0470846526.ch9, PMID: 9949805

Kramnik I, Dietrich WF, Demant P, Bloom BR. 2000. Genetic control of resistance to experimental infection with virulent *Mycobacterium tuberculosis*. *PNAS* **97**:8560–8565. DOI: https://doi.org/10.1073/pnas.150227197, PMID: 10890913

Leal IS, Smedegård B, Andersen P, Appelberg R. 2001. Failure to induce enhanced protection against tuberculosis by increasing T-cell-dependent interferon-γ generation. *Immunology* **104**:157–161. DOI: https://doi.org/10.1046/j.1365-2567.2001.01305.x

Lindenstrøm T, Knudsen NPH, Agger EM, Andersen P. 2013. Control of chronic *Mycobacterium tuberculosis* infection by CD4 KLRG1- IL-2-secreting central memory cells. *Journal of Immunology* **190**:6311–6319. DOI: https://doi.org/10.4049/jimmunol.1300248, PMID: 23677471

Llibre A, Bilek N, Bondet V, Darboe F, Mbandi SK, Penn-Nicholson A, Hatherill M, Rozenberg F, Scriba TJ, Duffy D. 2019. Plasma type I IFN protein concentrations in human tuberculosis. *Frontiers in Cellular and Infection Microbiology* **9**:e0296. DOI: https://doi.org/10.3389/fcimb.2019.00296

Lönnroth K, Williams BG, Cegielski P, Dye C. 2010. A consistent log-linear relationship between tuberculosis incidence and body mass index. *International Journal of Epidemiology* **39**:149–155. DOI: https://doi.org/10.1093/ije/dyp308, PMID: 19820104

Lowe DM, Redford PS, Wilkinson RJ, O'Garra A, Martineau AR. 2012. Neutrophils in tuberculosis: friend or foe? *Trends in Immunology* **33**:14–25. DOI: https://doi.org/10.1016/j.it.2011.10.003, PMID: 22094048

Lyadova IV, Tsiganov EN, Kapina MA, Shepelkova GS, Sosunov VV, Radaeva TV, Majorov KB, Shmitova NS, van den Ham H-J, Ganusov VV, De Boer RJ, Racine R, Winslow GM. 2010. In mice, tuberculosis progression is associated with intensive inflammatory response and the accumulation of Gr-1 cells in the lungs. *PLOS ONE* **5**:e10469. DOI: https://doi.org/10.1371/journal.pone.0010469, PMID: 20454613

Majlessi L, Simsova M, Jarvis Z, Brodin P, Rojas M-J, Bauche C, Nouzé C, Ladant D, Cole ST, Sebo P, Leclerc C. 2006. An increase in antimycobacterial Th1-cell responses by prime-boost protocols of immunization does not enhance protection against tuberculosis. *Infection and Immunity* **74**:2128–2137. DOI: https://doi.org/10.1128/IAI.74.4.2128-2137.2006, PMID: 16552042

Manz MG, Boettcher S. 2014. Emergency granulopoiesis. *Nature Reviews. Immunology* **14**:302–314. DOI: https://doi.org/10.1038/nri3660, PMID: 24751955

Marzo E, Vilaplana C, Tapia G, Diaz J, Garcia V, Cardona PJ. 2014. Damaging role of neutrophilic infiltration in a mouse model of progressive tuberculosis. *Tuberculosis* **94**:55–64. DOI: https://doi.org/10.1016/j.tube.2013.09.004, PMID: 24291066

Mishra BB, Lovewell RR, Olive AJ, Zhang G, Wang W, Eugenin E, Smith CM, Phuah JY, Long JE, Dubuke ML, Palace SG, Goguen JD, Baker RE, Nambi S, Mishra R, Booty MG, Baer CE, Shaffer SA, Dartois V, McCormick BA, et al. 2017. Nitric oxide prevents a pathogen-permissive granulocytic inflammation during tuberculosis. *Nature Microbiology* **2**:17072. DOI: https://doi.org/10.1038/nmicrobiol.2017.72, PMID: 28504669

Mittrücker HW, Steinhoff U, Köhler A, Krause M, Lazar D, Mex P, Miekley D, Kaufmann SHE. 2007. Poor correlation between BCG vaccination-induced T cell responses and protection against tuberculosis. *PNAS* **104**:12434–12439. DOI: https://doi.org/10.1073/pnas.0703510104, PMID: 17640915

Moeller AH, Suzuki TA, Phifer-Rixey M, Nachman MW. 2018. Transmission modes of the mammalian gut microbiota. *Science* **362**:453–457. DOI: https://doi.org/10.1126/science.aat7164, PMID: 30361372

Mogues T, Goodrich ME, Ryan L, LaCourse R, North RJ. 2001. The relative importance of T cell subsets in immunity and immunopathology of airborne *Mycobacterium tuberculosis* infection in mice. *The Journal of Experimental Medicine* **193**:271–280. DOI: https://doi.org/10.1084/jem.193.3.271, PMID: 11157048

Moreira-Teixeira L, Stimpson PJ, Stavropoulos E, Hadebe S, Chakravarty P, Ioannou M, Aramburu IV, Herbert E, Priestnall SL, Suarez-Bonnet A, Sousa J, Fonseca KL, Wang Q, Vashakidze S, Rodríguez-Martínez P, Vilaplana C, Saraiva M, Papayannopoulos V, O'Garra A. 2020a. Type I IFN exacerbates disease in tuberculosis-susceptible mice by inducing neutrophil-mediated lung inflammation and NETosis. *Nature Communications* **11**:5566. DOI: https://doi.org/10.1038/s41467-020-19412-6, PMID: 33149141

Moreira-Teixeira L, Tabone O, Graham CM, Singhania A, Stavropoulos E, Redford PS, Chakravarty P, Priestnall SL, Suarez-Bonnet A, Herbert E, Mayer-Barber KD, Sher A, Fonseca KL, Sousa J, Cá B, Verma R, Haldar P, Saraiva M, O'Garra A. 2020b. Mouse transcriptome reveals potential signatures of protection and pathogenesis in human tuberculosis. *Nature Immunology* **21**:464–476. DOI: https://doi.org/10.1038/s41590-020-0610-z, PMID: 32205882

Nair S, Huynh JP, Lampropoulou V, Loginicheva E, Esaulova E, Gounder AP, Boon ACM, Schwarzkopf EA, Bradstreet TR, Edelson BT, Artyomov MN, Stallings CL, Diamond MS. 2018. Irg1 expression in myeloid cells prevents immunopathology during *M. tuberculosis* Infection. *The Journal of Experimental Medicine* **215**:1035–1045. DOI: https://doi.org/10.1084/jem.20180118, PMID: 29511063

Nandi B, Behar SM. 2011. Regulation of neutrophils by interferon-γ limits lung inflammation during tuberculosis infection. *The Journal of Experimental Medicine* **208**:2251–2262. DOI: https://doi.org/10.1084/jem.20110919, PMID: 21967766

Niazi MKK, Dhulekar N, Schmidt D, Major S, Cooper R, Abeijon C, Gatti DM, Kramnik I, Yener B, Gurcan M, Beamer G. 2015. Lung necrosis and neutrophils reflect common pathways of susceptibility to *Mycobacterium tuberculosis* in genetically diverse, immune-competent mice. *Disease Models & Mechanisms* **8**:1141–1153. DOI: https://doi.org/10.1242/dmm.020867, PMID: 26204894

Nogueira BMF, Krishnan S, Barreto-Duarte B, Araújo-Pereira M, Queiroz ATL, Ellner JJ, Salgame P, Scriba TJ, Sterling TR, Gupta A, Andrade BB. 2022. Diagnostic biomarkers for active tuberculosis: progress and challenges. *EMBO Molecular Medicine* **14**:e14088. DOI: https://doi.org/10.15252/emmm.202114088, PMID: 36314872

Pan H, Yan B-S, Rojas M, Shebzukhov YV, Zhou H, Kobzik L, Higgins DE, Daly MJ, Bloom BR, Kramnik I. 2005. Ipr1 gene mediates innate immunity to tuberculosis. *Nature* **434**:767–772. DOI: https://doi.org/10.1038/nature03419, PMID: 15815631

Phifer-Rixey M, Bi K, Ferris KG, Sheehan MJ, Lin D, Mack KL, Keeble SM, Suzuki TA, Good JM, Nachman MW. 2018. The genomic basis of environmental adaptation in house mice. *PLOS Genetics* **14**:e1007672. DOI: https://doi.org/10.1371/journal.pgen.1007672, PMID: 30248095

Qu HQ, Li Q, McCormick JB, Fisher-Hoch SP. 2011. What did we learn from the genome-wide association study for tuberculosis susceptibility? *Journal of Medical Genetics* **48**:217–218. DOI: https://doi.org/10.1136/jmg.2010.087361, PMID: 21239447

Ravesloot-Chávez MM, Van Dis E, Stanley SA. 2021. The innate immune response to *Mycobacterium tuberculosis* infection. *Annual Review of Immunology* **39**:611–637. DOI: https://doi.org/10.1146/annurev-immunol-093019-010426, PMID: 33637017

Rothchild AC, Jayaraman P, Nunes-Alves C, Behar SM. 2014. iNKT cell production of GM-CSF controls *Mycobacterium tuberculosis*. *PLOS Pathogens* **10**:e1003805. DOI: https://doi.org/10.1371/journal.ppat.1003805, PMID: 24391492

Rothchild AC, Stowell B, Goyal G, Nunes-Alves C, Yang Q, Papavinasasundaram K, Sassetti CM, Dranoff G, Chen X, Lee J, Behar SM. 2017. Role of granulocyte-macrophage colony-stimulating factor production by T cells during *Mycobacterium tuberculosis* infection. *mBio* **8**:e01514-17. DOI: https://doi.org/10.1128/mBio.01514-17, PMID: 29066547

Sakai S, Kauffman KD, Schenkel JM, McBerry CC, Mayer-Barber KD, Masopust D, Barber DL. 2014. Cutting edge: control of *Mycobacterium tuberculosis* infection by a subset of lung parenchyma-homing CD4 T cells. *Journal of Immunology* **192**:2965–2969. DOI: https://doi.org/10.4049/jimmunol.1400019, PMID: 24591367

Sakai S, Kauffman KD, Sallin MA, Sharpe AH, Young HA, Ganusov VV, Barber DL. 2016. CD4 T cell-derived IFN-γ Plays a minimal role in control of pulmonary *Mycobacterium tuberculosis* infection and must be actively

repressed by PD-1 to prevent lethal disease. *PLOS Pathogens* **12**:e1005667. DOI: https://doi.org/10.1371/journal.ppat.1005667, PMID: 27244558

Salcedo T, Geraldes A, Nachman MW. 2007. Nucleotide variation in wild and inbred mice. *Genetics* **177**:2277–2291. DOI: https://doi.org/10.1534/genetics.107.079988, PMID: 18073432

Scanga CA, Mohan VP, Yu K, Joseph H, Tanaka K, Chan J, Flynn JL. 2000. Depletion of CD4(+) T cells causes reactivation of murine persistent tuberculosis despite continued expression of interferon gamma and nitric oxide synthase 2. *The Journal of Experimental Medicine* **192**:347–358. DOI: https://doi.org/10.1084/jem.192.3.347, PMID: 10934223

Scott NR, Swanson RV, Al-Hammadi N, Domingo-Gonzalez R, Rangel-Moreno J, Kriel BA, Bucsan AN, Das S, Ahmed M, Mehra S, Treerat P, Cruz-Lagunas A, Jimenez-Alvarez L, Muñoz-Torrico M, Bobadilla-Lozoya K, Vogl T, Walzl G, du Plessis N, Kaushal D, Scriba TJ, et al. 2020. S100A8/A9 regulates CD11b expression and neutrophil recruitment during chronic tuberculosis. *The Journal of Clinical Investigation* **130**:3098–3112. DOI: https://doi.org/10.1172/JCI130546, PMID: 32134742

Scriba TJ, Penn-Nicholson A, Shankar S, Hraha T, Thompson EG, Sterling D, Nemes E, Darboe F, Suliman S, Amon LM, Mahomed H, Erasmus M, Whatney W, Johnson JL, Boom WH, Hatherill M, Valvo J, De Groote MA, Ochsner UA, Aderem A, et al. 2017. Sequential inflammatory processes define human progression from *M. tuberculosis* infection to tuberculosis disease. *PLOS Pathogens* **13**:e1006687. DOI: https://doi.org/10.1371/journal.ppat.1006687, PMID: 29145483

Silvin A, Chapuis N, Dunsmore G, Goubet AG, Dubuisson A, Derosa L, Almire C, Hénon C, Kosmider O, Droin N, Rameau P, Catelain C, Alfaro A, Dussiau C, Friedrich C, Sourdeau E, Marin N, Szwebel TA, Cantin D, Mouthon L, et al. 2020. Elevated calprotectin and abnormal myeloid cell subsets discriminate severe from mild COVID-19. *Cell* **182**:1401–1418. DOI: https://doi.org/10.1016/j.cell.2020.08.002, PMID: 32810439

Singhania A, Verma R, Graham CM, Lee J, Tran T, Richardson M, Lecine P, Leissner P, Berry MPR, Wilkinson RJ, Kaiser K, Rodrigue M, Woltmann G, Haldar P, O'Garra A. 2018. A modular transcriptional signature identifies phenotypic heterogeneity of human tuberculosis infection. *Nature Communications* **9**:2308. DOI: https://doi.org/10.1038/s41467-018-04579-w, PMID: 29921861

Smith CM, Proulx MK, Olive AJ, Laddy D, Mishra BB, Moss C, Gutierrez NM, Bellerose MM, Barreira-Silva P, Phuah JY, Baker RE, Behar SM, Kornfeld H, Evans TG, Beamer G, Sassetti CM. 2016. Tuberculosis susceptibility and vaccine protection are independently controlled by host genotype. *mBio* **7**:e01516-16. DOI: https://doi.org/10.1128/mBio.01516-16, PMID: 27651361

Smith CM, Proulx MK, Lai R, Kiritsy MC, Bell TA, Hock P, Pardo-Manuel de Villena F, Ferris MT, Baker RE, Behar SM, Sassetti CM. 2019. Functionally overlapping variants control tuberculosis susceptibility in collaborative cross mice. *mBio* **10**:e02791-19. DOI: https://doi.org/10.1128/mBio.02791-19, PMID: 31772048

Smith CM, Baker RE, Proulx MK, Mishra BB, Long JE, Park SW, Lee HN, Kiritsy MC, Bellerose MM, Olive AJ, Murphy KC, Papavinasasundaram K, Boehm FJ, Reames CJ, Meade RK, Hampton BK, Linnertz CL, Shaw GD, Hock P, Bell TA, et al. 2022. Host-pathogen genetic interactions underlie tuberculosis susceptibility in genetically diverse mice. *eLife* **11**:e74419. DOI: https://doi.org/10.7554/eLife.74419, PMID: 35112666

Srivastava S, Ernst JD, Desvignes L. 2014. Beyond macrophages: the diversity of mononuclear cells in tuberculosis. *Immunological Reviews* **262**:179–192. DOI: https://doi.org/10.1111/imr.12217, PMID: 25319335

Stanley SA, Johndrow JE, Manzanillo P, Cox JS. 2007. The Type I IFN response to infection with *Mycobacterium tuberculosis* requires ESX-1-mediated secretion and contributes to pathogenesis. *Journal of Immunology* **178**:3143–3152. DOI: https://doi.org/10.4049/jimmunol.178.5.3143, PMID: 17312162

Suzuki TA, Martins FM, Phifer-Rixey M, Nachman MW. 2020. The gut microbiota and Bergmann's rule in wild house mice. *Molecular Ecology* **29**:2300–2311. DOI: https://doi.org/10.1111/mec.15476, PMID: 32419280

Svenson KL, Gatti DM, Valdar W, Welsh CE, Cheng R, Chesler EJ, Palmer AA, McMillan L, Churchill GA. 2012. High-resolution genetic mapping using the Mouse Diversity outbred population. *Genetics* **190**:437–447. DOI: https://doi.org/10.1534/genetics.111.132597, PMID: 22345611

Tait DR, Hatherill M, Van Der Meeren O, Ginsberg AM, Van Brakel E, Salaun B, Scriba TJ, Akite EJ, Ayles HM, Bollaerts A, Demoitié M-A, Diacon A, Evans TG, Gillard P, Hellström E, Innes JC, Lempicki M, Malahleha M, Martinson N, Mesia Vela D, et al. 2019. Final analysis of a trial of M72/AS01$_E$ vaccine to prevent tuberculosis. *The New England Journal of Medicine* **381**:2429–2439. DOI: https://doi.org/10.1056/NEJMoa1909953, PMID: 31661198

Tameris MD, Hatherill M, Landry BS, Scriba TJ, Snowden MA, Lockhart S, Shea JE, McClain JB, Hussey GD, Hanekom WA, Mahomed H, McShane H, MVA85A 020 Trial Study Team. 2013. Safety and efficacy of MVA85A, a new tuberculosis vaccine, in infants previously vaccinated with BCG: a randomised, placebo-controlled phase 2b trial. *Lancet* **381**:1021–1028. DOI: https://doi.org/10.1016/S0140-6736(13)60177-4, PMID: 23391465

Tan Y, Cahan P. 2019. SingleCellNet: A computational tool to classify single cell RNA-Seq data across platforms and across species. *Cell Systems* **9**:207–213. DOI: https://doi.org/10.1016/j.cels.2019.06.004, PMID: 31377170

Udeh R, Advani S, de Guadiana Romualdo LG, Dolja-Gore X. 2021. Calprotectin, an emerging biomarker of interest in COVID-19: A systematic review and meta-analysis. *Journal of Clinical Medicine* **10**:775. DOI: https://doi.org/10.3390/jcm10040775, PMID: 33672040

Van Dis E, Fox DM, Morrison HM, Fines DM, Babirye JP, McCann LH, Rawal S, Cox JS, Stanley SA. 2022. IFN-γ-independent control of *M. tuberculosis* requires CD4 T cell-derived GM-CSF and activation of HIF-1α. *PLOS Pathogens* **18**:e1010721. DOI: https://doi.org/10.1371/journal.ppat.1010721, PMID: 35877763

Xie X, Shi Q, Wu P, Zhang X, Kambara H, Su J, Yu H, Park SY, Guo R, Ren Q, Zhang S, Xu Y, Silberstein LE, Cheng T, Ma F, Li C, Luo HR. 2020. Single-cell transcriptome profiling reveals neutrophil heterogeneity in

homeostasis and infection. *Nature Immunology* **21**:1119–1133. DOI: https://doi.org/10.1038/s41590-020-0736-z, PMID: 32719519

Yang H, Wang JR, Didion JP, Buus RJ, Bell TA, Welsh CE, Bonhomme F, Yu AHT, Nachman MW, Pialek J, Tucker P, Boursot P, McMillan L, Churchill GA, de Villena FPM. 2011. Subspecific origin and haplotype diversity in the laboratory mouse. *Nature Genetics* **43**:648–655. DOI: https://doi.org/10.1038/ng.847, PMID: 21623374

Zak DE, Penn-Nicholson A, Scriba TJ, Thompson E, Suliman S, Amon LM, Mahomed H, Erasmus M, Whatney W, Hussey GD, Abrahams D, Kafaar F, Hawkridge T, Verver S, Hughes EJ, Ota M, Sutherland J, Howe R, Dockrell HM, Boom WH, et al. 2016. A blood RNA signature for tuberculosis disease risk: a prospective cohort study. *Lancet* **387**:2312–2322. DOI: https://doi.org/10.1016/S0140-6736(15)01316-1, PMID: 27017310